



VCU

Virginia Commonwealth University
VCU Scholars Compass

Theses and Dissertations

Graduate School

2016

Assessment of changes in the size of periapical radiolucencies 3-12 months post non-surgical root canal treatment using CBCT imaging: A pilot study

Jeremy W. Fike DDS
Virginia Commonwealth University

Follow this and additional works at: <https://scholarscompass.vcu.edu/etd>



Part of the [Endodontics and Endodontology Commons](#)

© The Author

Downloaded from

<https://scholarscompass.vcu.edu/etd/4139>

This Thesis is brought to you for free and open access by the Graduate School at VCU Scholars Compass. It has been accepted for inclusion in Theses and Dissertations by an authorized administrator of VCU Scholars Compass. For more information, please contact libcompass@vcu.edu.

© Jeremy W Fike, DDS 2016

All Rights Reserved

Assessment of changes in the size of periapical radiolucencies 3-12 months post
non-surgical root canal treatment using CBCT imaging: A pilot study

A thesis submitted in partial fulfillment of the requirements for the degree of Master of Science
in Dentistry at Virginia Commonwealth University

by

Jeremy W. Fike,
BS, Abilene Christian University, 2005
DDS, Texas A&M University Baylor College of Dentistry, 2011

Thesis Director: Karan J. Replogle, DDS, MS
Assistant Professor, Advanced Specialty Education Program in Endodontics

Virginia Commonwealth University
Richmond, Virginia
May 2016

Table of Contents

List of Tables	iii
List of Figures	iv
Introduction.....	1
Materials and Methods.....	15
Results.....	19
Discussion.....	44
Appendix A.....	52
Appendix B.....	59
Appendix C.....	60
Appendix D.....	62
Appendix E.....	69
Appendix F.....	75
References.....	79
Vita.....	85

List of Tables

1. Teeth in the Study	20
2. Pre-op and Recall Volumes Calculated by the Linear Measurements.....	25
3. Pre-op and Recall Di-Thresh Gui Volumes	25
4. Agreement on Change in Volume.....	29
5. Descriptive Statistics of the Linear Measurements.....	31
6. Descriptive Statistics for Area	34
7. Descriptive Statistics for the DTG measurements	38

List of Figures

1. Distribution of DTG Volume Measurements	21
2. Change in Pre-op and Recall DTG Volumes Measurements.....	21
3. Pre-op and Recall Volumes Calculated by the Linear Measurements.....	23
4. Change in Pre-op and Recall Volumes Calculated by the Linear Measurements	24
5. Correlation Between the Volume Measurements	27
6. Correlation Between the Recall vs Post-Op Ratios	28
7. Relationships Between the Linear Measurements	32
8. Relationships Between Area Calculations	35
9. Volume Calculated from Linear Measurements	36
10. Relationships Between Three Areas and Volume	37
11. Relationships Between the DTG measurements.....	39
12. Relationships Between the DTG diameters and volume	40
13. Calculated Ellipsoidal Volume By VOL (voxels)	41
14. Relationship Between the Mean and the SD.....	42
15. Cube Root of Volume	43

Abstract

ASSESSMENT OF CHANGES IN THE SIZE OF PERIAPICAL RADIOLUCENCIES 3-12 MONTHS POST NON-SURGICAL ROOT CANAL TREATMENT USING CBCT IMAGING: A PILOT STUDY

Jeremy Ward Fike, DDS

A thesis submitted in partial fulfillment of the requirements for the degree of Master of Science in Dentistry at Virginia Commonwealth University

Virginia Commonwealth University 2016

Director: Karan J. Replogle, DDS, MS
Assistant Professor, Advanced Specialty Education Program in Endodontics

The purpose of this study was to assess the changes in size of periapical lesions 3-12 months following root canal treatment using CBCT. Patients who had non-surgical root canal therapy (NSRCT) or non-surgical retreatment (ReTx) from July 30, 2014 to August 19, 2015 with a periapical lesion of endodontic origin and received NSRCT or ReTx and had a pre-treatment or intra-treatment CBCT were invited to participate. Volumetric and linear measurements of periapical lesions on initial and post-treatment CBCT images were performed. A total of 20 patients with 23 treated teeth with 30 separate periapical radiolucent lesions returned for follow up 91-390 days after the initiation of endodontic treatment. Lesions showed an overall reduction in volume ($p=0.0096$), maximum coronal diameter ($p=0.0117$), maximum sagittal diameter ($p=0.0071$), and maximum axial diameter ($p=0.0006$). Lesions show a significant reduction in size 3-12 months following non-surgical endodontic treatment using CBCT.

Introduction

The goal of endodontic treatment is to prevent or treat apical periodontitis. Apical periodontitis is an inflammatory disease at the root end of teeth. Prevalence studies show that by age 50 half of the population will have experienced the disease (1). The primary cause of apical periodontitis involves necrosis of dental pulp tissue with subsequent colonization by microorganisms. The host's immuno-inflammatory response to the presence of microorganisms and microbial byproducts in the pulp space of root canals induces pathological changes at the apex of teeth, inevitably leading to apical periodontitis (2, 3). As a result of apical periodontitis, several different types of lesions can develop at the apex of teeth. These lesions are referred to as periapical lesions.

In a typical situation, as dental caries approaches the coronal pulp tissue an acute inflammatory response within the pulp tissue occurs. Without therapeutic intervention, this inflammatory response results in the development of areas of necrotic tissue within the coronal pulp. With time, microorganisms colonize the necrotic tissue. Early in the inflammatory process a gradient within the pulp tissue is established. Areas of necrotic, infected tissue exist adjacent to areas with acute inflammation, which will in turn be adjacent to areas with chronic inflammation. A region of uninflamed vital pulp tissue follows. A tissue gradient is formed and the progression of pulp tissue necrosis with subsequent microbial colonization proceeds in an apical direction.

Contrary to widely held opinion it is not necessary for both the coronal and radicular pulp tissue to be necrotic and infected for a periapical lesion to develop (4-6). Pathological changes within the periapical tissues are usually not caused by the microorganisms themselves but rather by the microbial byproducts and toxins that diffuse through inflamed pulpal tissue to the periapex

as the microbial infection progresses apically within the root canal system. The immune response of the periapical tissues includes both innate and adaptive immune responses to the microbial produced irritants. Host defenses are not capable of eradicating the infection established in the necrotic pulp because of a lack of circulation to the areas of pulpal necrosis.

Morphologically, lesions of apical periodontitis manifest in different ways. A relatively simple way to subdivide these lesions is to place them in the categories of exudative and proliferative lesions. An example of an exudative lesion is an apical abscess. Examples of proliferative lesions include both apical granulomas and apical cysts. In reality a complex variety of transition stages and tissue configurations can exist between these various lesions. For example, in one of the first studies attempting to classify periradicular lesions, Thoma (7) classified lesions attached to extracted teeth as “simple dental granulomas,” “dental granulomas with epithelium,” “dental granulomas showing necrosis and suppuration,” “dental granulomas showing various retrograde processes”, and “dental granulomas showing the formation of cysts.”

Ricucci and others (6, 8-9) have suggested that histological diagnosis of lesions of apical periodontitis can only be made when the biopsy sample includes the root apex of the involved tooth, is in its original spatial relationship and is biopsied and sectioned meticulously with serial sectioning along the longitudinal axis of the sample. This type of tissue sample allows for differentiation of *true cysts* from *pocket cysts*. However, this type of biopsy sample is only obtainable by extracting teeth with an intact lesion or block resection of a root apex with an attached lesion during apical surgery.

Multiple studies have been performed to determine the prevalence of the various types of periradicular lesions. These studies have varied widely in their findings. For example, the prevalence of apical cysts ranges from 6% - 55% depending upon the author (9). This variation is

largely the result of differences in methods of tissue sampling and histological criteria. Nair's study utilizing 256 teeth extracted with intact periapical lesions, serial sectioning of the samples, and strict histological criteria concluded that 50% were periapical granulomas, 35% were periapical abscesses and 15% were periapical cysts (9). Ricucci's study involving 50 apical periodontitis lesions, found that 40% were granulomas, 32% were periapical cysts, and 28% were periapical abscesses. Both studies adhered to strict histological criteria and are two frequently cited studies regarding prevalence. However, Ricucci himself said, when commenting on both studies, that the studies "cannot automatically be regarded as corresponding to the actual prevalence in the general population (10)."

The clinical diagnosis of apical periodontitis is based upon signs and symptoms, the results of endodontic testing (pulp tests, percussion, palpation), and radiographic findings. In 2009, the American Association of Endodontists recommended diagnostic terminology for the clinical diagnosis of apical periodontitis (11). This classification system is primarily concerned with the presence of or lack of symptoms as well as clinical findings such as sinus tracts and intraoral or extraoral swelling as a result of odontogenic infections. These clinical diagnoses are crucial to the delivery of appropriate clinical care but they are not without their limitations.

For example, it is known that pulpitis can exist without symptoms (12) and that this pulpal inflammation can progress to necrosis without the patient experiencing pain (13). Similarly, apical periodontitis can be symptomatic or asymptomatic. Consequently, there is no correlation between the histopathologic findings of lesions of apical periodontitis and the clinical diagnosis (14, 15). When the patient's history, endodontic testing, and current signs and symptoms are inconclusive then clinical diagnosis has relied heavily on radiographic findings.

Radiography plays an essential role in diagnosis, treatment, and evaluation of outcome of teeth with apical periodontitis. A characteristic feature of apical periodontitis is bone loss around the tooth's apex. However, radiography is capable of detecting changes only when bone tissue has been lost due to apical periodontitis. It cannot detect the pathological changes at a cellular level prior to this event. Lesions of apical periodontitis are soft tissues that occupy the periapical space that was previously occupied by bone tissue. The radiographic findings of apical periodontitis have been repeatedly shown to have a poor correlation with the histopathological features of lesions of apical periodontitis (16, 17).

The host's immunological response to the infected tooth is both protective and destructive. The development of lesions of apical periodontitis is protective preventing microorganism from leaving the root of the tooth and spreading systemically. However, it is also destructive. The same biomolecules and host defense cells that are capable of destroying and damaging microbial cells are also capable of destroying and damaging host cells. The primary goal of therapeutic intervention in endodontics is to eliminate, or significantly reduce, the number of microorganisms colonizing the canal space. If this balance between microorganisms in the root canal space and immunological response is offset by a reduction in the number of microorganisms then healing of the apical tissues takes place.

Healing involves restitution of lost or damaged tissue and restoration of some of the original structures that were present before the injury took place (18). Healing occurs in four phases, hemostasis, inflammation, proliferation, and tissue remodeling. The phases are integrated and occur simultaneously (19).

Hemostasis occurs immediately after wounding and is the first phase of healing. It is characterized by vascular constriction and fibrin clot formation. Pro-inflammatory cytokines and

growth factors are present in the clot. Factors such as transforming growth factor (TGF)- β , platelet-derived growth factor (PDGF), fibroblast growth factor (FGF), and epidermal growth factor (EGF) play critical roles in the healing events that follow hemostasis (20).

In the inflammatory phase of healing polymorphonuclear neutrophils (PMNs) and monocytes migrate to the site. PMNs are capable of phagocytosis. Their primary role is removal of microbial cells. Monocytes are blood-borne cells capable of differentiation into macrophages. Both resident macrophages and newly differentiated macrophages play essential roles in phagocytizing debris, residual bacteria, and apoptotic tissue from the wound site.

During the proliferative phase, a migration of host cells, including fibroblasts and endothelial cells, occurs. These cells regenerate connective tissue and provide vascular support for the wound site. This process blends seamlessly with the final phase of healing, the remodeling phase. It is important to note that the remodeling phase may take months or years to complete.

The healing of apical periodontitis following nonsurgical root canal therapy follows these same events. After the removal or reduction of microorganisms, the inflammatory cytokines and mediators within the lesion undergo a shift from a proinflammatory, destructive nature to an anti-inflammatory and proliferative nature. Osteoprogenitor cells on the periphery of the lesion can then undergo differentiation into osteoblasts capable of secreting boney matrix to replace the bone lost by the lesion of apical periodontitis. In healing, the normal balance between bone forming osteoblasts and bone resorbing osteoclasts shifts towards an increase in bone formation.

Healing of apical periodontitis occurs from the peripheral tissues toward the center. Most of the new trabecular bone is endosteal in origin. If the cortical plate was affected by the disease, the periosteum participates in regeneration of the new cortical bone. The last tissue to repair may

be the periodontal ligament (10). Cementum is capable of proliferation to cover the areas where cementum was damaged or lost on the root end.

Ricucci (10) has pointed out the sequence of healing events is hypothetical since no study has clearly shown all of these events. Current information comes largely from observations and studies involving the repair of tissues following tooth extraction and apical surgery, as well as animal studies and cross-sectional observations in humans whose teeth with healing lesions were extracted for reasons such as fracture or prosthetic planning (10).

Following the completion of therapeutic interventions, histological data is not available to the clinician to assess the healing or non-healing of apical periodontitis. Consequently, evaluation of lesion size by radiograph has been essential to the evaluation of lesions post-operatively. In addition to the absence of symptoms, swelling, and sinus tracts, complete restitution of the lamina dura and periodontal ligament (PDL) space on post operative radiograph has been considered the optimal outcome following nonsurgical root canal therapy.

In 1956, Strindberg (21), published a strict criteria for successful endodontic treatment that included complete radiographic resolution of the apical lesion. Orstavik's classic study in 1996 of 599 endodontically treated roots (22) showed that the peak incidence of healing of apical periodontitis was one year following treatment. However, he noted that in some cases four years or more may be necessary for complete healing as evidenced on radiographs. This study formed the basis for the European Society of Endodontology's recommendation that the first follow-up examination should be made one year after treatment and that if the lesion has failed to resolve, further follow-up appointments should be completed every year for a period of four years (23). The Society went further to suggest that if a radiolucency has persisted for four years or longer the case should be classified as a failure, even in the absence of clinical signs and symptoms.

Currently, periapical lesions are commonly evaluated using periapical radiographs within a clinical setting (24). On a periapical radiograph, a lesion will be represented by radiolucency at the tooth's apex. Pre-operative periapical radiographs are used to estimate the size and extent of periapical lesions prior to treatment. Post-operative periapical radiographs are used to detect the change in size of periapical lesions following endodontic treatment. A decrease in size or complete disappearance of the periapical lesion following treatment is indicative of healing, whereas, an increase in size of a lesion may be indicative of a non-healing lesion due to persistent disease. When the post-operative lesion is the same size as the pre-operative lesion the results are uncertain. This situation can occur if the post-operative radiograph is taken early in the healing process. Dimensional changes in periapical lesions often cannot be detected on periapical radiographs for at least 6-12 months following the completion of endodontic therapy (22, 25-26).

The outcome of the endodontic treatment, lesion healing, may not be known for one year or more following completion of treatment. Cone Beam Computed Tomography (CBCT) overcomes several of the limitations of periapical radiographs. It is hypothesized that CBCT may be capable of detecting dimensional changes in lesions at an earlier point in time than periapical radiographs.

In 1991 Walter K. Murphy, an Oral and Maxillofacial Surgery resident at the Medical College of Virginia, published a study evaluating the healing of periapical radiolucencies after nonsurgical endodontic therapy using conventional periapical radiographs (26). Murphy's retrospective chart review evaluated healing in 89 patients. The inclusion criteria included patients with diagnostic pretreatment and post-treatment periapical radiographs. The patients all originally presented with a periapical radiolucency measuring at least 2mm in both an apical-

occlusal and mesiodistal dimension on a periapical radiograph. The patients had no history of endodontic surgery on the tooth in question and a minimum of three months of follow-up after completion of nonsurgical endodontic therapy. The study found that 41 (46.1%) of the periapical lesions had resolved at the time of follow up and 43 (48.3%) had undergone partial radiographic resolution, meaning the periapical radiolucency had decreased in size.

In addition, the study (26) found that the length of follow-up was a significant factor. If the follow up occurred 12 months after nonsurgical endodontic treatment, 70.6% of the lesion demonstrated complete healing, whereas, if the recall period was six months or less only 17.6% showed complete resolution. The article (26) also discussed the limitations of periapical radiographs. It explicitly states that a source of error in the study involved the measurement of lesions in only two dimensions. Identified was the impossibility of evaluating the bucco-lingual extent of lesions. At that time the clinician was limited to two-dimensional evaluation of such lesions.

Periapical radiographs have several known limitations. Radiographs show a two dimensional representation of a three dimensional lesion. The presence of anatomical structures, including but not limited to, cortical and cancellous bone, the maxillary sinus, and neurovascular tissue, can make interpretation of periapical lesions difficult (27). Bender and Seltzer reported that periapical lesions could not be detected if they are confined solely to cancellous bone (28) or have not resulted in more than 12.5% total bone loss in the area (29). Other authors have refuted these findings (30, 31), noting that lesions can be detected radiographically without perforation of the cortical bone. However, there is agreement that lesion location influences radiographic visualization and it is known that the width of buccal bone varies with anatomical region (32). There is also agreement that cortical bone loss enhances visualization radiographically (33).

Cone beam computed tomography (CBCT) is a three-dimensional imaging technique that has been shown to overcome several of the known limitations of periapical radiographs (34-37). CBCT is capable of detecting lesions that cannot be detected on periapical radiographs, including but not limited to, lesions of small size (38), and lesions that are confined solely to cancellous bone (39). CBCT images show lesions in three dimensions and allow for measurement of the area of low density (PARL) to give a very accurate estimate of actual lesion size (40).

Cone-beam technology has existed in the medical field since the 1980s (27). In the late 1990s a new tomographic scanner, known as cone beam computed tomography (CBCT), was developed specifically for dental and maxillofacial use (41). The Food and Drug Administration approved the first CBCT unit for dental use in the United States in March 2001(42). Since that time the use of CBCT technology in endodontics has increased worldwide (24). Cotton et al recommended that graduate endodontic programs incorporate training in CBCT technology in 2007 (43) and Patel et al reiterated that recommendation in a review article in 2015 (24). Today, most, if not all endodontic residency programs in the United States utilize CBCT. It is widely recognized as a technology that will have a large impact on endodontics in the future.

CBCT produces three-dimensional scans of the maxilla-facial skeleton using an extra-oral system. Cone-beam technology uses a cone-shaped beam of radiation. The radiation source and detector rotate between 180 and 360 degrees around the patient's head to obtain the image (44). Voxels are 3-D cubes of information that represent a value on a regular grid in three-dimensional space. All the voxels are isotropic, which means they are a perfect three-dimensional cube. This enables objects within the scan volume to be measured accurately in multiple planes (43).

CBCT is generally classified into limited or full field of views (FOV). Limited FOV's scans range in diameter from 40-100mm, while the full FOV scans range from 100-200mm (43). Additionally, smaller FOVs generally allow for smaller voxel sizes (0.1-0.2mm vs 0.3-0.4mm). Smaller voxel sizes offer higher resolution (43). An additional benefit of limited FOV's is the decreased radiation dose to the patient. The images can be viewed in the axial, coronal (or facial), and sagittal planes and three-dimensional reconstruction is possible with computer software. In endodontics, a focused view CBCT is considered to be the preferred FOV as it improves diagnostic accuracy, decreases radiation exposure to the patient, is a smaller volume to interpret and focuses on the anatomical areas of interest (45).

Widening of the periodontal ligament space is the earliest periapical finding on radiographs suggestive of apical pathosis. The average width of the periodontal ligament space is 200um. Therefore, it has been suggested that optimal resolution of any CBCT imaging system used in endodontics not exceed 200um (42, 46).

There are three basic dose units in radiation dosimetry (41). The *radiation absorbed dose* is the amount of energy absorbed from the radiation beam per unit mass of tissue. This is measured in joules per kilogram. How dangerous a given type of radiation might be or how radiosensitive the particular irradiated tissue is not considered in the definition (41). The *equivalent dose* is obtained by multiplying the *radiation-absorbed dose* by a radiation-quality weighting factor. This factor accounts for the differing amounts of tissue damage that can result from the same amount of different types of radiation (41). Finally, the *effective dose* is obtained by multiplying the *equivalent dose* by different tissue weighting factors. The tissue weighting factors take into account that different tissues have differing levels or radiosensitivity (41).

In maxillofacial imaging the micro Sievert [10^{-6} Sieverts : μSv] is typically used to quantify the radiation dose. The effective dose of radiation can be compared among different imaging modalities. In the head and neck region, the radiation exposure to the bone marrow, thyroid, esophagus, skin, bone surface, salivary glands, and brain are of particular interest (47).

It is estimated that one day of background radiation at sea level is 7-8 μSv (47). One digital periapical radiograph has an estimated effective dose of 6 μSv (47). This means that one digital periapical radiograph is equal to approximately one day of equivalent background radiation. CBCT images differ in the effective dose of radiation based upon multiple factors including the exposure settings of the CBCT scanner, the size of the FOV, exposure time, tube current and the energy/potential (24). The effective dose is also based upon the area of the oral cavity within the FOV (24). For a focused field CBCT in the maxillary or mandibular anterior the effective dose is estimated to be 4.7 μSv or 21.7 μSv , respectively (48). For a focused field CBCT in the maxillary posterior the effective dose is estimated to be 9.8 μSv (48). For a focused field CBCT in the mandibular posterior the effective dose is estimated to be 38.3 μSv (48).

CBCT has been used as an aid in a variety of endodontic situations. These situations include, but are not limited to, assessment of apical periodontitis, detection of vertical root fractures, assessment of root canal anatomy, pre-surgical assessment, diagnosis and management of root resorption, and dental trauma (24). It has been suggested that the assessment of treatment outcome is a potential application of CBCT technology (41).

The lack of well-designed clinical trials and subsequent meta-analysis regarding CBCT use in endodontics, mean that currently decisions regarding the use of CBCT for different endodontic applications are largely empirical (24). In an effort to provide clinicians with the best scientifically based guidance available, the American Association of Endodontists (AAE) and the

American Academy of Oral and Maxillofacial Radiology (AAOMR) released a joint statement in 2015 that provided recommendations for the use of CBCT in endodontics (49). The position paper recommended that intraoral radiographs be considered the imaging modality of choice for the evaluation of endodontic patients and immediate postoperative imaging. It recommended that Limited FOV CBCT be considered the imaging modality of choice for cases that are difficult to diagnose with radiographs alone, for preoperative imaging of teeth with suspected complex morphology, identification of calcified canals, evaluating the non-healing of previous endodontic treatment, assessment of treatment complications prior to non-surgical re-treatment, pre-surgical treatment planning, assessment of vertical root fractures (VRF), dental implant placement, diagnosis and management of dento-alveolar trauma, and localization and differentiation of external and internal resorptive defects.

In his 2014 CBCT review article, Patel et al specifically suggested that future clinical research trials, using small FOV CBCT scans, should be done to assess the healing of lesions associated with apical periodontitis. Since CBCTs are capable of detecting periapical lesions at smaller sizes than periapical radiographs (38, 39), and capable of more accurate estimates of actual lesion sizes (40), logic would lead to a hypothesis that CBCTs may be capable of detecting dimensional changes in lesions at an earlier point in time than periapical radiographs.

Multiple methodologies have been employed to evaluate bone healing including but not limited to radiographic subtraction techniques (51, 52), ultrasound (53, 54), MRI (44), tuned aperture computed tomography (55, 56), computed tomography (57, 58), and CBCT (43). However, within endodontics periapical radiographs are by far the most common way to assess healing of periapical lesions following endodontic treatment (22).

Since CBCT is capable of allowing assessment of lesions in three dimensions it has been suggested that volumetric measurements of lesions may be a way to assess dimensional change (59). Several authors have found volumetric measurements to be highly correlated with actual physical volumes of artificially created bone lesions (35, 60). The first clinical study to assess 3-dimensional volumetric changes of periapical lesions after root canal treatment was published by van der Borden in 2013 (61). Subsequently investigations by Liang et al, Metska et al and Zhang et al have used CBCT to assess healing of lesions of apical periodontitis using volumetric measurements (62-64).

The first clinical study that used volumetric measurement of periapical lesions on CBCT to assess outcome was published in 2013 in the Journal of Endodontics (61). In this study 50 teeth having 71 roots with evidence of periapical bone loss, were recalled 10-37 months following treatment. The study evaluated outcome by comparing initial lesion sizes on both periapical radiographs and CBCT with post-operative images. At recall, 11 of 71 roots (15.5%) showed complete resolution of the lesion on CBCT compared with 32 of 71 (45.1%) on periapical radiograph. Overall, 55 of 71 roots (77.5%) showed a reduction in lesion size compared with 63 of 71 roots (88.7%) on periapical radiograph. The study concluded that lesion changes after root canal treatment determined with 3D volumetric CBCT data and 2-dimensional PA data were different.

Also in 2013, Liang et al examined 84 single-rooted teeth associated with periapical lesions 10-19 months after non-surgical root canal treatment (64). The change in lesion size was assessed using both PAs and CBCT. A volumetric measurement was made of both the pre-operative and post-operative lesion. The study found that CBCT detected significantly more

post-treatment lesions than PA. Overall an absence of a radiolucent lesion on CBCT was observed in 16 of 84 teeth (19%) and a reduction was observed in 61 of 84 teeth (72.6%).

In 2015, Zhang et al looked at 61 single rooted teeth that had a periapical radiolucent lesion present on a CBCT one year following endodontic treatment (62). A second CBCT image was obtained 2 years following endodontic treatment. Their study showed that the volume of the lesions decreased from 1-year post operatively to 2 years in 38 of 61 teeth (63%). The volume remained unchanged in 20 of 61 (33%) and the volume increased in 2 of 61 teeth (3%). They concluded that healing of apical periodontitis is a dynamic process that takes time.

Metska was the first to apply a volumetric assessment of lesion size on CBCT to cases treated by orthograde retreatment (63). The study evaluated 45 root filled teeth with persistent apical periodontitis that required non-surgical retreatment. Two CBCT images were obtained for each patient, the first taken prior to treatment and a second taken one year following retreatment. The volume of the periapical lesions decreased in 20 teeth (57%), remained unchanged in 8 (23%), and increased in 7 (20%).

To our knowledge no study has evaluated the change in size of periapical radiolucencies using CBCT less than 10 months following endodontic treatment. The aim of this study was to evaluate the change in periapical lesion size using CBCT 3-12 months following non-surgical endodontic treatment.

Materials and Methods

This study utilized a review of secondary data using a prospective cohort design to determine the dimensional changes that occur in periapical radiolucencies using CBCT 3-12 months following nonsurgical root canal therapy. The VCU Institutional Review Board approved the study (IRB #HM20003014). Eligible for inclusion were all patients referred to the Graduate Endodontic Practice at Virginia Commonwealth University School of Dentistry for NSRCT or ReTx from July 30, 2014 through August 19, 2015.

Graduate endodontic residents completed the initial evaluations of all patients. Evaluation included subjective and objective information, clinical findings, diagnostic test results and pulpal and periapical diagnoses. This information was recorded in the electronic patient record (Axium©). Treatment options were reviewed with the patients and included: 1) perform NSRCT or retreatment, 2) extract the tooth and replace with prosthesis (i.e. fixed partial denture, implant and crown, or removable partial denture), and 3) do no further treatment. The advantages, disadvantages, risks, benefits, and cost of these treatment options were discussed with the patient.

Specifically the following data was recorded:

Subjective Symptoms: Pain to Cold, Pain to Heat, Pain on Biting or Release, Localizable or Diffuse Pain

Diagnostic Testing: Cold test, Bite test (Biting and Release), Percussion test, Transillumination, Mobility, and Probing Depths

Radiographic Evaluation: Presence or Absence of Periapical Radiolucency, Size of the Periapical Radiolucency, Periodontal Defects Present (Isolated, Generalized, or Vertical)

Diagnosis:

Pulpal: Symptomatic Irreversible Pulpitis, Asymptomatic Irreversible Pulpitis, Pulpal Necrosis, Previously Treated

Periapical: Normal Periapical Tissues, Symptomatic Apical Periodontitis, Asymptomatic Apical Periodontitis, Acute Apical Abscess, Chronic Apical Abscess

Non-surgical root canal therapy (NSRCT) or non-surgical retreatment (ReTx) was performed using standard clinical protocol. Instrumentation was performed using stainless steel hand files and a variety of different nickel titanium rotary systems. Irrigation included 5.25% Sodium Hypochlorite and 17% Ethylenediaminetetraacetic acid (EDTA) for all cases. In some cases 2% chlorhexidine was used. All canals were cleaned and shaped to a minimum of a 30/.04 final apical diameter. Obturation was performed with gutta percha using either cold lateral condensation or a continuous wave warm vertical technique. Roth's 401® sealer or Tubliseal® was used. Following obturation the access opening was occluded using a provisional material, (Interim Restorative Material (IRM®) or Cavit®) or definitively restored (resin composite or amalgam). All cases were performed using a Ziess® OPMI Pico microscope.

Patients were included in the study if NSRCT or ReTx was completed on one of their teeth and if a pre-treatment or intra-treatment CBCT showed an area of low density (PARL) around the apex of at least one root of the tooth in question. An area of low density (or radiolucency) around a root was defined as a PARL if it measured more than twice the width of the normal periodontal ligament space on an adjacent healthy tooth.

Documentation of the patient's clinical records had to be complete for inclusion. Patients who were pregnant, had a history of receiving therapeutic radiation to the head or neck, were younger than 18 or older than 89, were excluded from the study. Any teeth that had a history of endodontic surgery were excluded. There was no restriction for race, ethnicity, or sex.

It is standard practice that all patients are enrolled in the post endodontic treatment recall system in the graduate practice. Patients who met the inclusion criteria were asked to return to the graduate practice for a recall appointment. The recall included a clinical and radiographic evaluation for the tooth in question. Patients were given information about the study and asked if they would like to participate. If patients were interested in participation they were given a copy of the study consent form to read and sign. Participants were compensated \$10 in cash. For participants, a follow-up CBCT was obtained. No clinical protocol was altered for the sake of the study.

All the CBCT scans, both initial and follow-up, were taken with the Carestream 9300 system (Carestream Health; Rochester, NY). All CBCT images were taken using a limited field of view (5 x 5 cm) and a voxel size of 0.090 mm. Operating parameters were set at 2-10mA, 60-90 kV, and 12 seconds. CBCT images were analyzed using a Dell Optiplex 990 computer (Dell SA, Geneva, Switzerland) and a 22-inch LCD monitor with a resolution of 1680 x 1050 pixels (Dell SA, Geneva, Switzerland). All preoperative images were taken to aid the resident in diagnosis and treatment of the case.

Each periapical radiolucency was measured by an endodontic resident using DiThreshGUI software (DiThreshGUI 1.4). DiThreshGUI software was developed by Anthony Fouad. It uses a 2 plane cross-correlation method to determine the volume, maximum coronal diameter, maximum sagittal diameter, and maximum axial diameter of periapical lesions. Each lesion was measured 3 times (DiThreshGui lesion measurement protocol, Appendix A). Data from each measurement was compiled using Microsoft Excel (Microsoft Corp. Redmond, WA).

A board-certified oral and maxillofacial radiologist and board-certified endodontist performed linear measurements on each periapical radiolucency using Carestream 3D Imaging

software (Carestream Health; Rochester, NY). Each evaluator was given a copy of the Protocol for Lesion Measurement (see Appendix B). Using orthogonal slicing, the evaluator located the slice that appeared to demonstrate the largest area of the lesion and made a measurement of the lesion at what appeared to be the widest dimension. A second measurement was then made at 90 degrees to this initial measurement. The evaluator was asked to make a measure from a bone landmark to another bone landmark. If the lesion did not have clearly demarcated boney borders, for example if the cortical plate was perforated by the lesion or if the sinus was perforated by the lesion, the evaluator was asked to estimate the lesion boundary based upon the bone that could be observed on either side of the bone defect. These measurements were performed in the axial, coronal, and sagittal planes for each lesion. A calibration between examiners was performed by comparing the measurements made on the first 5 lesions in the study.

After the evaluator made the measurements of the pre-operative or intra-operative scan and the post-operative scan, the evaluator then observed both scans on two adjacent monitors and made an evaluation of the change in lesion size using a 3 point Likert scale.

Results

The study population comprised patients who presented for endodontic treatment in the Graduate Endodontic Practice at VCU School of Dentistry (Richmond, VA). Patients were referred for evaluation and treatment from the VCU School of Dentistry undergraduate student clinics as well as the AEGD residency, Faculty Practice, and Richmond metropolitan private dental practices. All patients had NSRCT or ReTx completed in the graduate endodontic practice at VCU.

Forty-two patients were identified as having met the inclusion criteria; 7 patients declined because of personal reasons and 1 patient moved out of the state. Four patients scheduled follow-up visits but did not show up for their appointments. Ten patients could not be reached by phone despite numerous attempts to contact them for recall visits. Twenty patients returned for recall appointments and consented to participation in the study. The recall rate was 47.6%

The participants (n=20) had an average age of 50.7 (SD = 18.5, range = 21 to 78). They had a total of 23 treated teeth with 30 separate periapical radiolucent lesions. The patients returned 91-390 days following the initiation of their endodontic treatment. Ten patients (13 teeth, 18 separate periapical lesions) were recalled 6 months or less following the initiation of treatment (91-153 days). Ten patients (10 teeth, 12 separate periapical lesions) were recalled (241-390 days). Complete data compiled for the 20 participants and 30 separate periapical lesions can be found in Appendix C.

Table 1. Teeth in the Study

Tooth Type		Count		
		Mandibular	Maxillary	Total
Incisor	L1	0	3	3
	L2	0	1	1
Premolar	P1	1	3	4
	P2	0	1	1
Molar	M1	6	6	12
	M2	1	1	2

The volumetric data obtained from the DiThreshGui (DTG) software are show in Appendix D. Volume, maximum coronal diameter (MCD), maximum sagittal diameter (MSD), and maximum apical diameter (MAD) were determined. Using DiThreshGui software 21 lesions showed a reduction in volume of 20%+ at recall, 4 lesions showed an increase of 20% at recall, and 5 lesions showed a change of 12% or less at recall. A volumetric decrease in lesion size was seen as early as 91 days following the initiation of treatment.

The cube root of the triplicate DTG volume measurement were averaged and then back-transformed to the original scale. The DTG measurements of volume were strongly skewed. The pre-op volumes ranged from 3471 to 275,129 voxels with a median value of 87,263 voxels, which is less than the mean value of 110,260. The recall volumes ranged from 0 to 318,435 voxels with a median value of 41,732 voxels, which is less than the mean value of 64891 voxels. Figure 1 shows the distribution of the volume measurements on the two occasions and Figure 2 shows that the majority of the lesions decreased in volume.

In Figure 1 each dot represents a periapical radiolucency. Dots below the diagonal line showed a decrease in size and dots above the line showed an increase in size. In Figure 2 the change in volume is shown for each lesion. Specific time intervals are not identified.

Figure 1. Distribution of DTG Volume Measurements

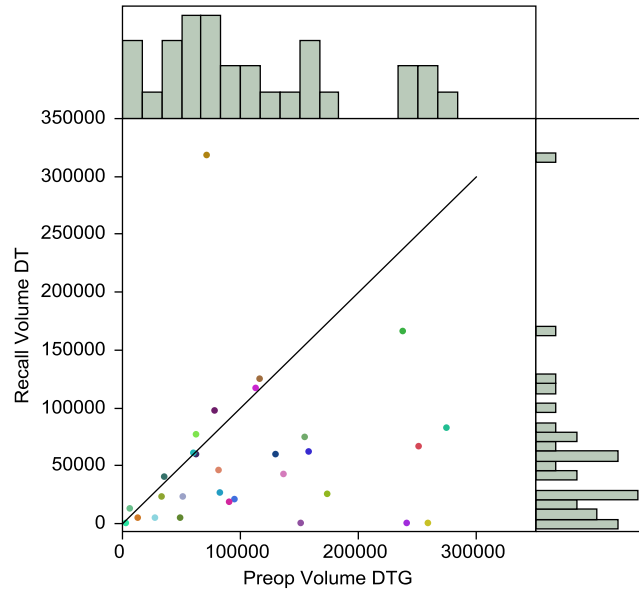
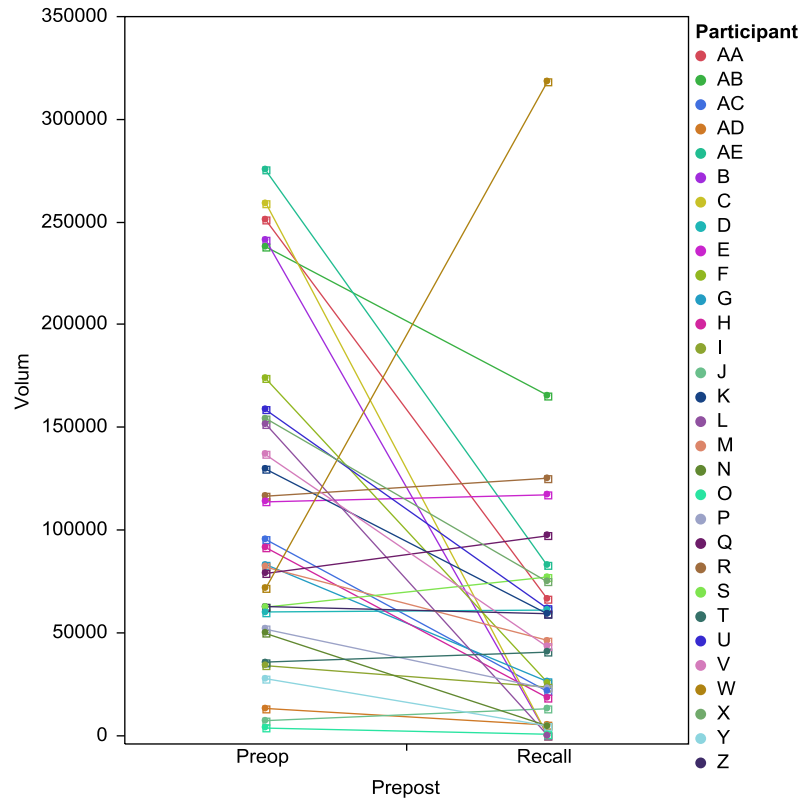


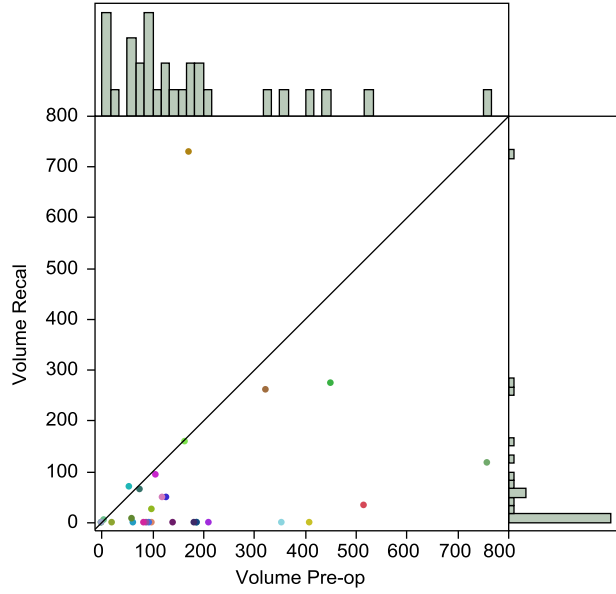
Figure 2. Change in Pre-op and Recall DTG Volumes Measurements



The linear measurements of the two evaluators can be found in Appendix E. The linear measurements were used to calculate the volume of the 30 lesions using the maximum diameters and an ellipsoid mathematical model. Like the volumes obtained using DTG, the volumes, obtained from the linear measurements, were strongly skewed. The pre-op volumes ranged from 0 to 758mm³ with a median value of 117 mm³, which is less than the mean value of 166 mm³. The recall volumes ranged from 0 to 730mm³ with a median value of 23 mm³, which is less than the mean value of 80 mm³. Figure 3 shows the distribution of the volume measurements on the two occasions, by examiner. Each lesion is colored to compare the measurements across the two panels. Lesions below the diagonal line decreased in size, and those few above the diagonal increased in size. The change in volume can be better seen in Figure 4. What is apparent is that most lesions decrease in size, but some remain the same size and the occasional one increases. Specific time intervals are not identified.

Figure 3. Pre-op and Recall Volumes Calculated by the Linear Measurements by Examiner

Radiologist



Endodontist

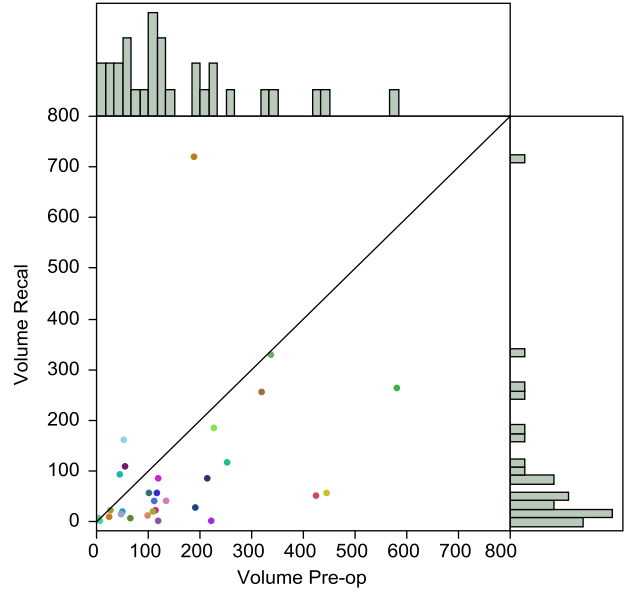
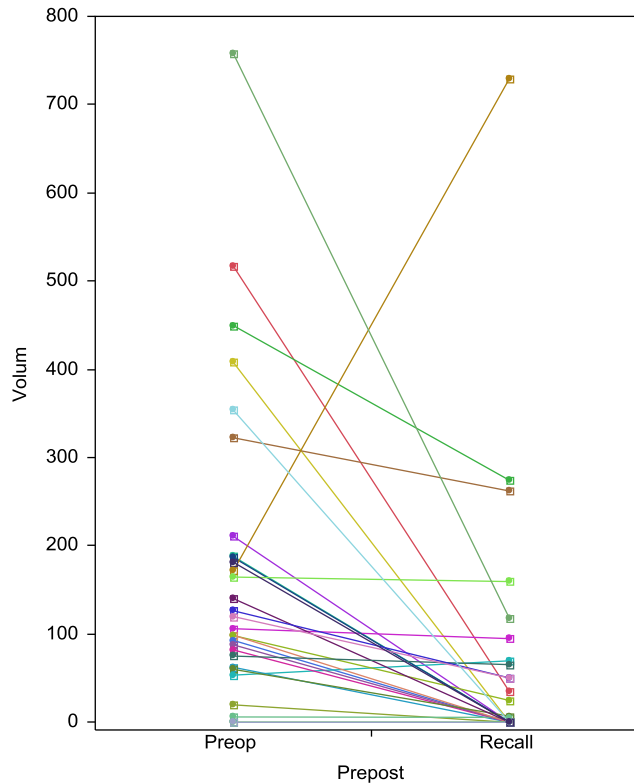
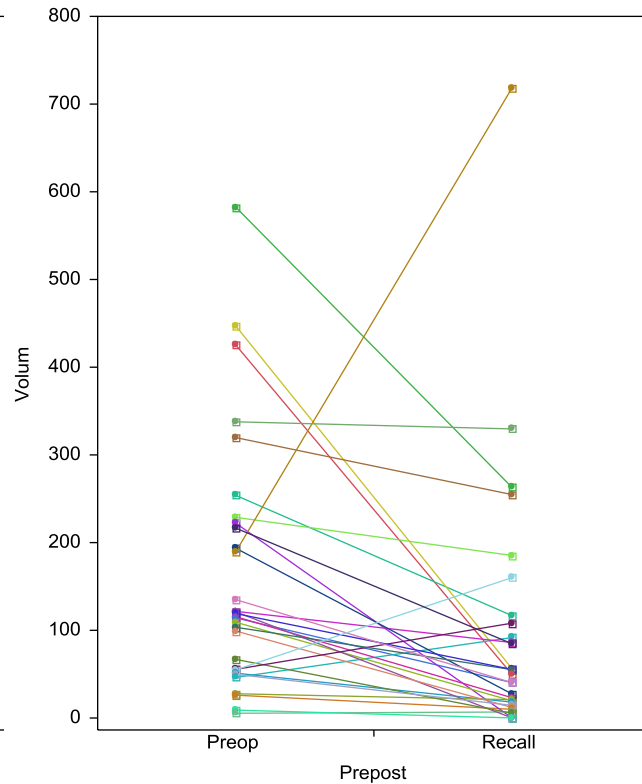


Figure 4. Change in Pre-op and Recall Volumes Calculated by the Linear Measurements by Examiner

Radiologist



Endodontist



To deal with the skewed values, the cube-root of the volume measurements were analyzed using repeated-measures mixed model ANOVA. Overall, the volumes significantly decreased ($P < .0001$, Table 2). However, the two examiners had different mean values ($P < .0001$) and, as a result, the amount of change from pre-op to recall varied by examiner ($P = 0.0053$). For the measurements obtained by the radiologist, the average volume decreased from 110mm^3 to 6.4mm^3 , a change of 94% ($P < .0001$). For the measurements obtained by the endodontist, the average volume decreased from 125mm^3 to 40mm^3 , a change of 68% ($P = .0006$).

Table 2. Pre-op and Recall Volumes Calculated by the Linear Measurements, Overall and by Examiner

Occasion	Volume	95%CI	P-value
Overall			
PreOp	117.51	(69.48 to 183.74)	
Recall	18.34	(4.77 to 46.32)	
Ratio	0.156		<.0001
Change	0.844		
Radiologist			
PreOp	109.90	(58.48 to 185.04)	
Recall	6.38	(0.43 to 25.87)	
Ratio	0.058		<.0001
Change	0.942		
Endodontist			
PreOp	125.47	(78.68 to 187.87)	
Recall	39.98	(15.67 to 81.54)	
Ratio	0.319		0.0006
Change	0.681		

A repeated-measures mixed-model ANOVA was performed on the cube-root transformation. Estimates were obtained by back-transforming the estimates.

Again, the cube-root of the volume measurements were analyzed using repeated-measures mixed model ANOVA. Overall, the volumes significantly decreased ($P < .0001$, Table 2). For the measurements obtained by the radiologist, the average volume decreased from 90964 voxels to 30,149 voxels, a change of 67% ($P = .0004$). The median change was 59%.

Table 3. Pre-op and Recall Di-Thresh Gui Volumes

Occasion	Volume	95%CI	P-value
PreOp	90964	(64635 to 123617)	
Recall	30149	(15719 to 51468)	
Ratio	0.33		0.0004
Change	0.67		

Three volumetric measurements were obtained. The volume obtained by the DTG software and the calculated volumes obtained by the radiologist's and endodontist's

measurements. In addition to the difference between the units (mm^3 vs. voxels), the measurement of volume is not identical by the three measurements. Figure 5 shows the correlations between the three measurements at pre-op and at recall. Note that the cube-root scale is used for all to make these measurements approximately normal and, thus, the correlations meaningful. All of the pre-op measurements are strongly correlated ($r > 0.72$) and all of the recall measurements are strongly correlated ($r > 0.68$). It's to be expected that the correlations across the two occasions are reduced. There also is substantial agreement between the recall vs post-op ratios as shown in Figure 6.

Figure 5. Correlation Between the Volume Measurements

Volume (cube root)	Preop DTG	Preop Radiologist	Preop Endodontist	Recall DTG	Recall Radiologist	Recall Endodontist
Preop DTG	1.00	0.72	0.83	0.17	0.17	0.22
Preop Radiologist	0.72	1.00	0.84	0.32	0.37	0.58
Preop Endodontist	0.83	0.84	1.00	0.33	0.41	0.50
Recall DTG	0.17	0.32	0.33	1.00	0.69	0.80
Recall Radiologist	0.17	0.37	0.41	0.69	1.00	0.70
Recall Endodontist	0.22	0.58	0.50	0.80	0.70	1.00

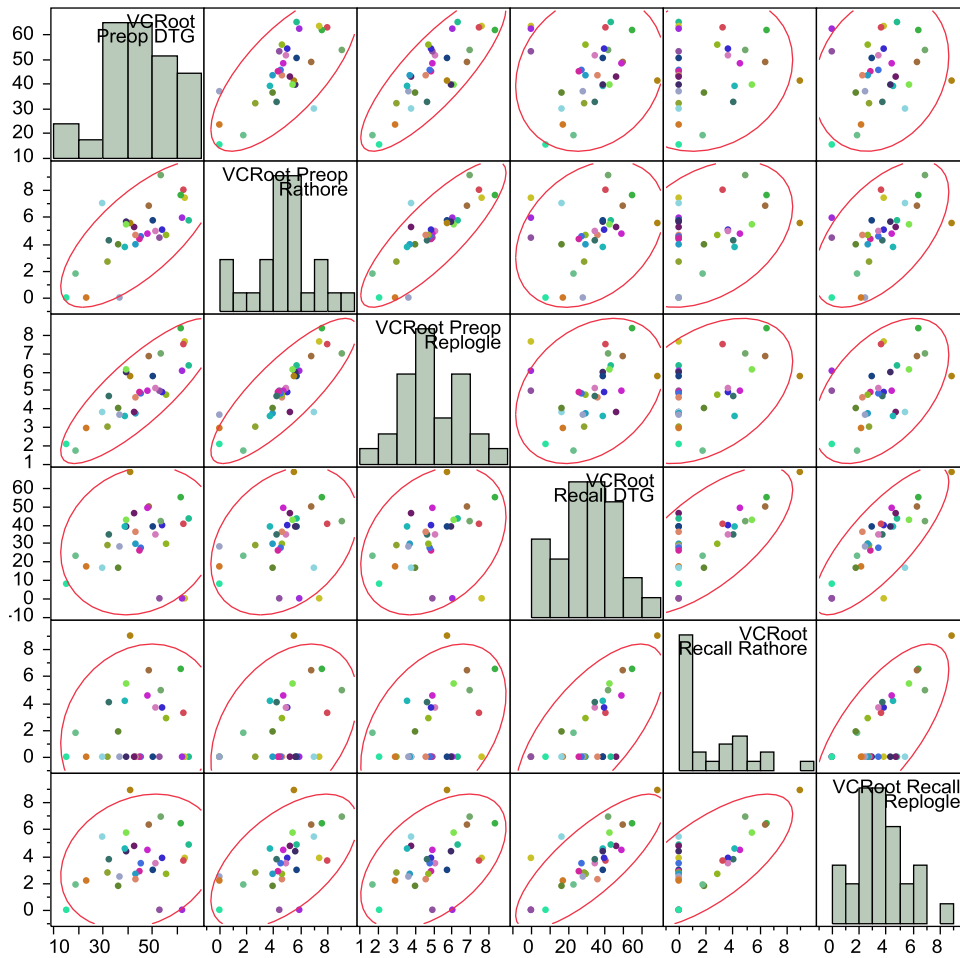
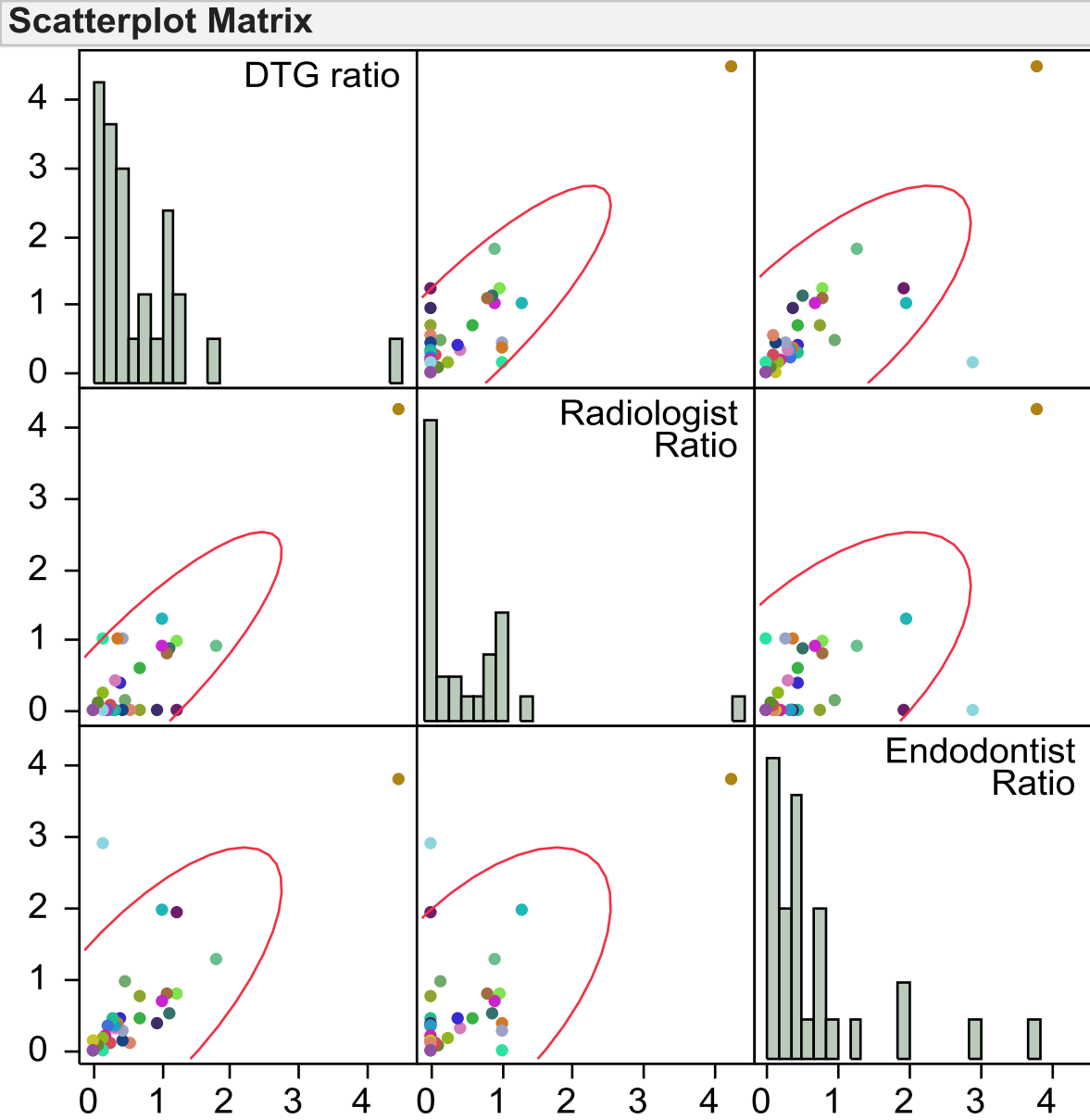


Figure 6. Correlation between the Recall vs Post-Op Ratios

Correlations			
	DTG ratio	Radiologist Ratio	Endodontist Ratio
DTG ratio	1.0000	0.8625	0.7366
Radiologist Ratio	0.8625	1.0000	0.6269
Endodontist Ratio	0.7366	0.6269	1.0000



After making the linear measurements, the two raters were asked to characterize the pair of readings as “Decreasing in size”, “Cannot see a change”, or “Increasing in size.” They agreed in 70% of the cases, with a significant chance-corrected agreement (Kappa = 47%, P = 0.0006, Table 4). Additional results using the Likert scale are in Appendix F.

Table 4. Agreement on Change in Volume

Endodontist	Radiologist			Total
	Decreasing in size	Cannot see a change	Increasing in size	
Decreasing in size	14	3	0	17
Cannot see a change	2	6	2	10
Increasing in size	0	2	1	3
Total	16	11	3	30

70% agreement; Kappa = 47.0% (P = 0.0006)

Generally, the Endodontist declared “Decreasing” if the recall lesion was less than 54% of the pre-op; “Cannot see a change” if the ratio was between 70% and 195% of the pre-op, and “Increasing” if the recall to pre-op ratio was 198% or above. The Radiologist declared “Decreasing” if the recall lesion was 100% or less of the pre-op, “Cannot see a change” if the ratio was below 130%, and “Increasing” for the case that was 425%.

Two examiners, a radiologist and an endodontist recorded the linear measurements. They each independently determined the largest width of the lesion on the axial view (Axial 1) and then determined the largest height perpendicular to this width (Axial 2). Then, in similar manner the Sagittal 1 and Sagittal 2 measurements were made and the Coronal 1 and Coronal 2 measurements made. On the nine occasions when the radiologist did not give a measurement, a zero value was used. The summary descriptive statistics for the measurements are shown in Table 5 and visually presented in measurements Figure 7. Figure 7 and the correlations indicate that all of the linear measurements are strongly related—that measuring “lesion size” in any view

will yield similar results. A multivariate ANOVA of the six measurements indicated that there was no significant difference between the two raters ($P = 0.2084$).

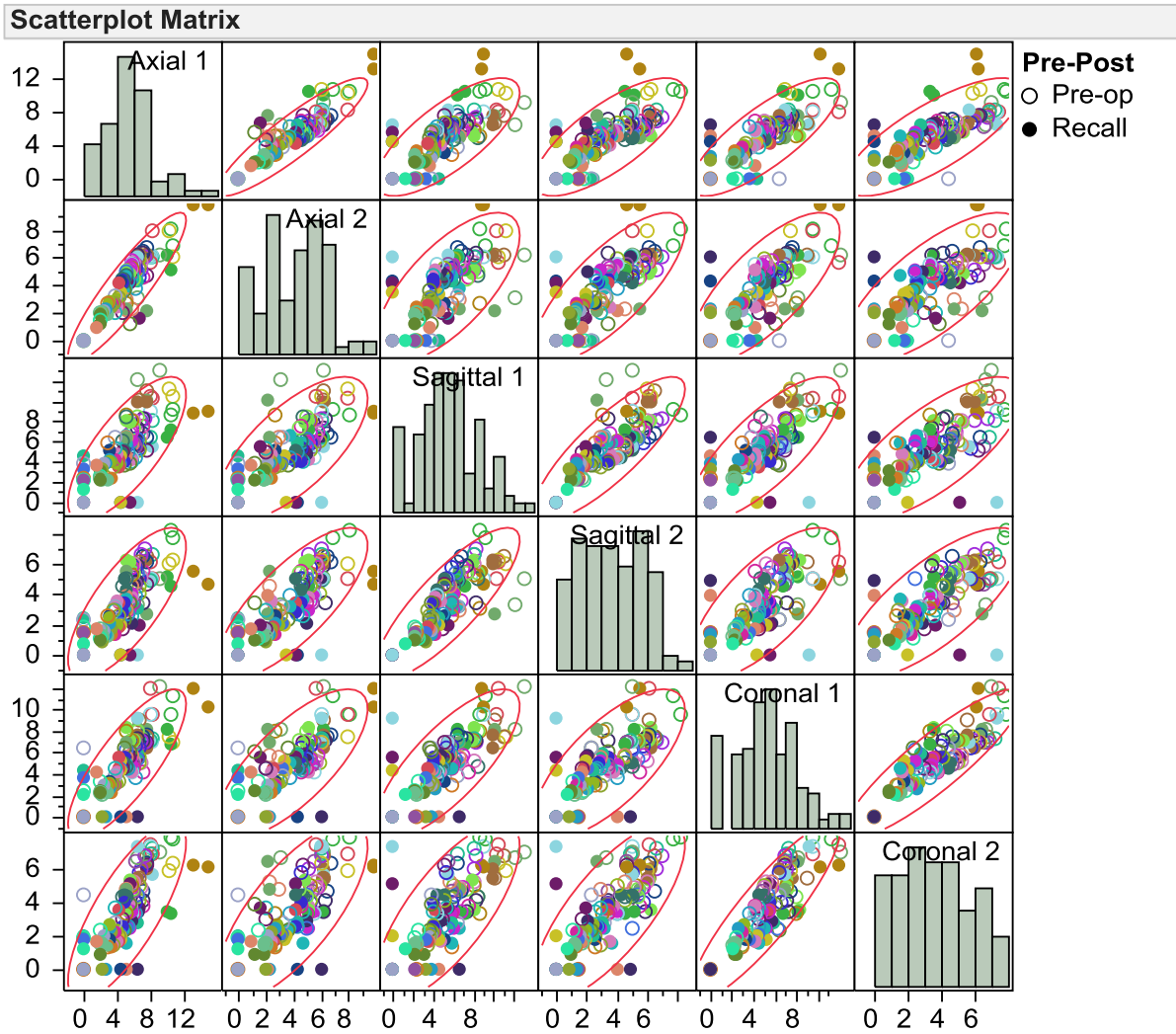
Table 5. Descriptive statistics of the linear measurements

Variable	Mean	Std Dev	Range	
Pre-op				
Axial 1	5.94	2.33	0	10.7
Axial 2	4.57	1.94	0	8.1
Sagittal 1	6.61	2.54	2.2	13.0
Sagittal 2	4.44	1.71	1.1	8.2
Coronal 1	6.09	2.36	0	12.1
Coronal 2	4.51	1.87	0	7.9
Recall				
Axial 1	4.25	3.14	0	14.8
Axial 2	3.17	2.32	0	9.8
Sagittal 1	4.09	2.76	0	10.1
Sagittal 2	2.51	1.91	0	6.3
Coronal 1	4.00	2.90	0	12.0
Coronal 2	2.48	1.98	0	7.3

Correlations

Variable	Axial 1	Axial 2	Sagittal 1	Sagittal 2	Coronal 1	Coronal 2
Axial 1	1.00	0.90	0.75	0.75	0.80	0.78
Axial 2	0.90	1.00	0.69	0.77	0.74	0.73
Sagittal 1	0.75	0.69	1.00	0.83	0.77	0.74
Sagittal 2	0.75	0.77	0.83	1.00	0.72	0.75
Coronal 1	0.80	0.74	0.77	0.72	1.00	0.89
Coronal 2	0.78	0.73	0.74	0.75	0.89	1.00

Figure 7. Relationships between the linear measurements

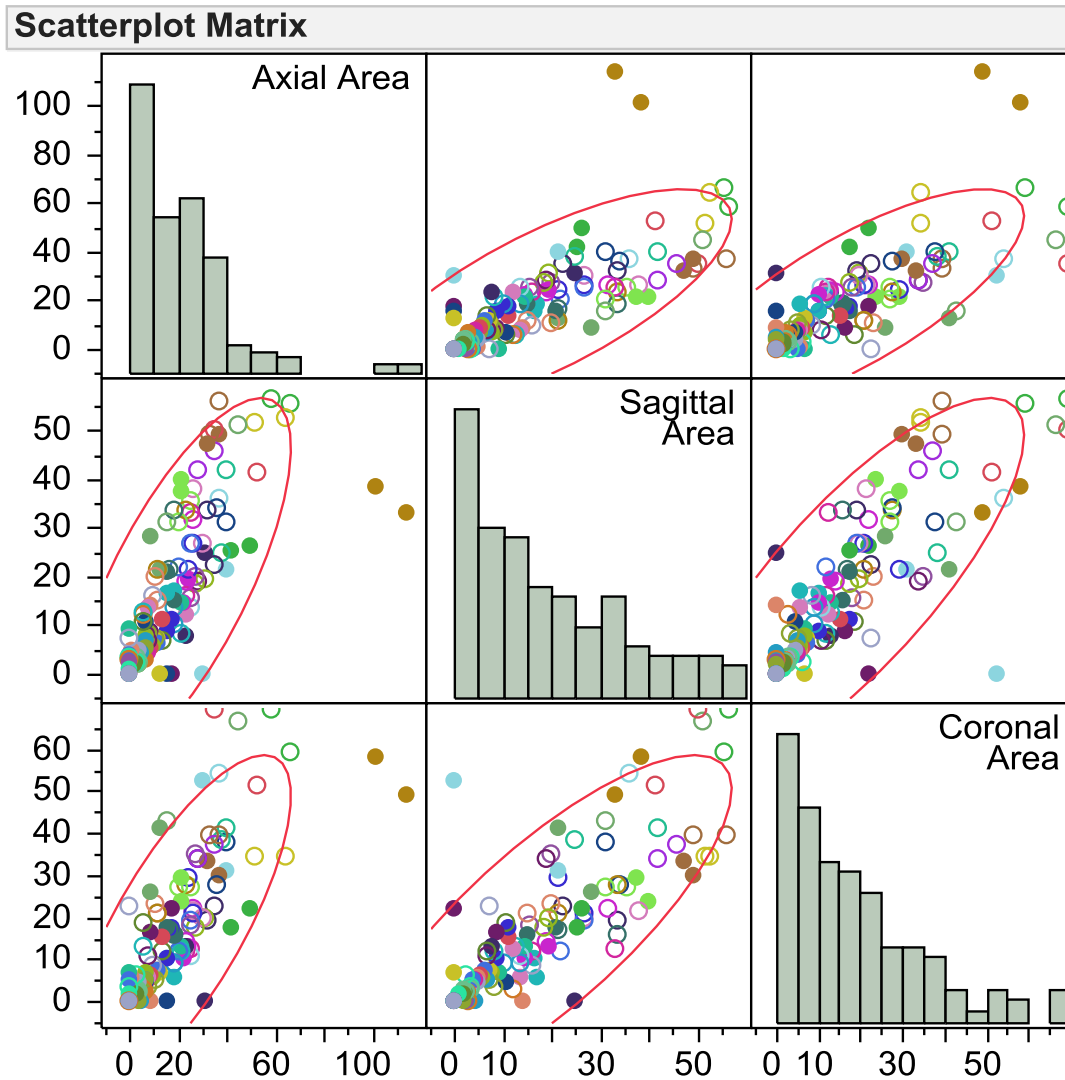


In each view, the coronal, sagittal and axial, the area of a lesion may be calculated. The area of an ellipse with the principle axes (radii) of length a , and b is Calculated Area = $\frac{\pi}{4}ab$. Using the linear measurements as twice the radii, area was calculated in the axial, sagittal, and coronal planes. The summary statistics for the three areas are shown in Table 6 and the relationships between the three are depicted in Figure 8. Note that all the areas are rather skewed; therefore, the summary statistics are affected by the outliers.

Table 6. Descriptive Statistics for Area

Variable	Mean	Std Dev	Range	
Pre-op				
Axial Area	24.35	15.50	0	66.16
Sagittal Area	25.32	15.66	2.2	56.36
Coronal Area	24.36	16.94	0	69.23
Recall				
Axial Area	15.71	20.89	0	113.91
Sagittal Area	11.66	12.60	0	49.48
Coronal Area	11.80	13.83	0	58.43
Correlations				
Variable	Axial Area	Sagittal Area	Coronal Area	
Axial Area	1.00	0.73	0.76	
Sagittal Area	0.73	1.00	0.80	
Coronal Area	0.76	0.80	1.00	

Figure 8. Relationships between Area Calculations



The volume of an ellipsoid with the principle axes (radii) of length a, b, and c is Calculated

$$\text{Volume} = \frac{4}{3} \pi abc .$$

Using the largest of the pair of diameters as twice the radii in this formula,

the volume may be calculated. As might be expected, volume is strongly skewed with a large number of very small (or zero) volumes and a few large volumes (Figure 9). The mean pre-op volume is 166.4mm³ and the median is lower, 117.2mm³. The mean recall volume is 79.9mm³ and the median is much lower, 23.8mm³.

Figure 9. Volume Calculated from Linear Measurements

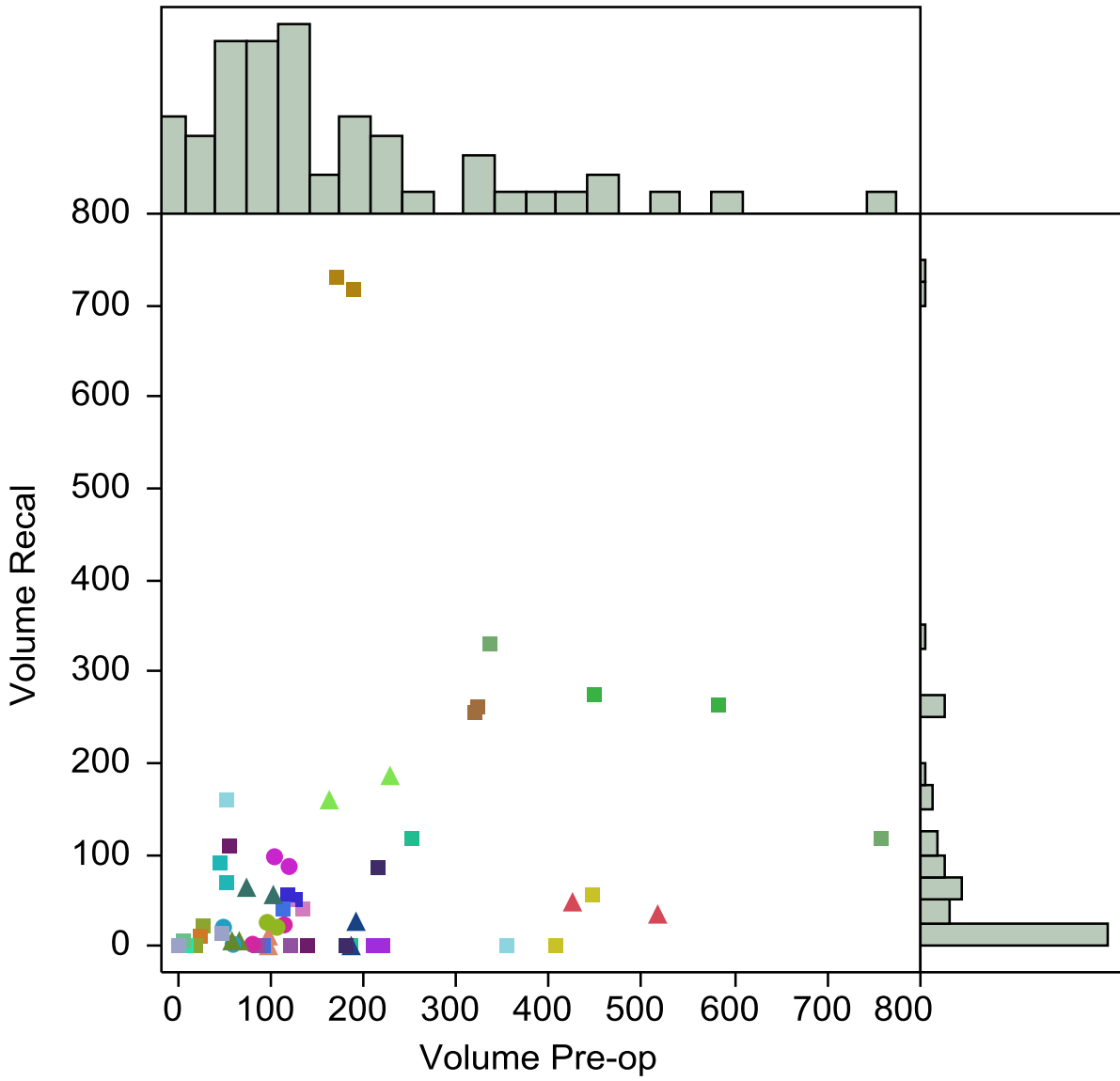
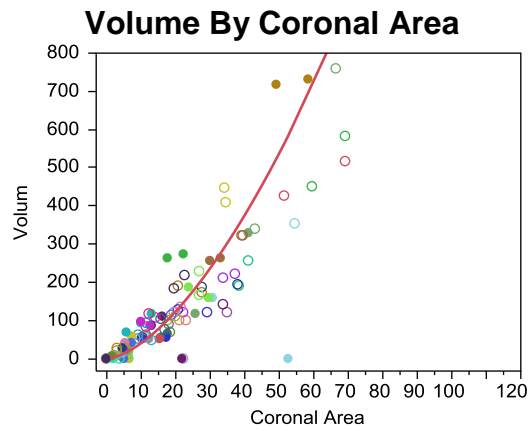
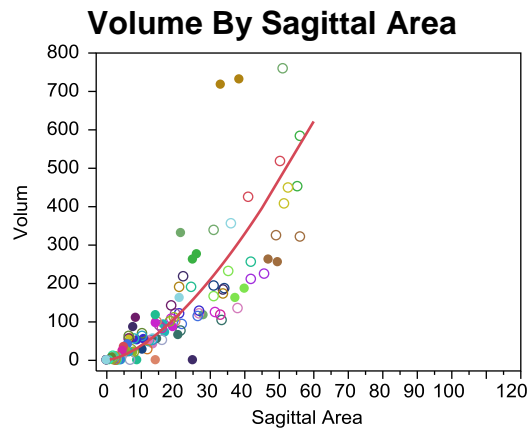
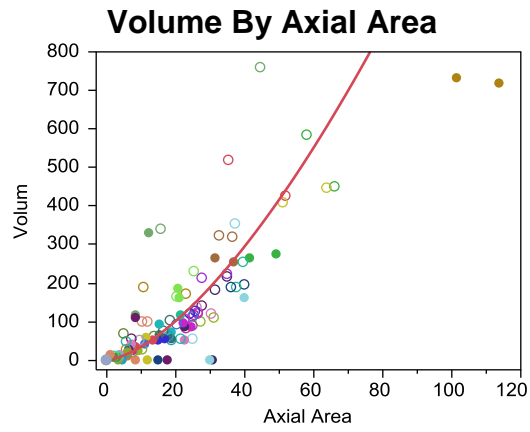


Figure 10. Relationships between Three Areas and Volume



Using the two linear measurements, an area was calculated using the ellipse for the measurements made in the axial, sagittal, and coronal views. These areas were compared with the volume of the lesion calculated using an ellipsoid model using the three largest measurements in the three planes, as previously described. Figure 10 shows the relationship between the three areas and calculated volume.

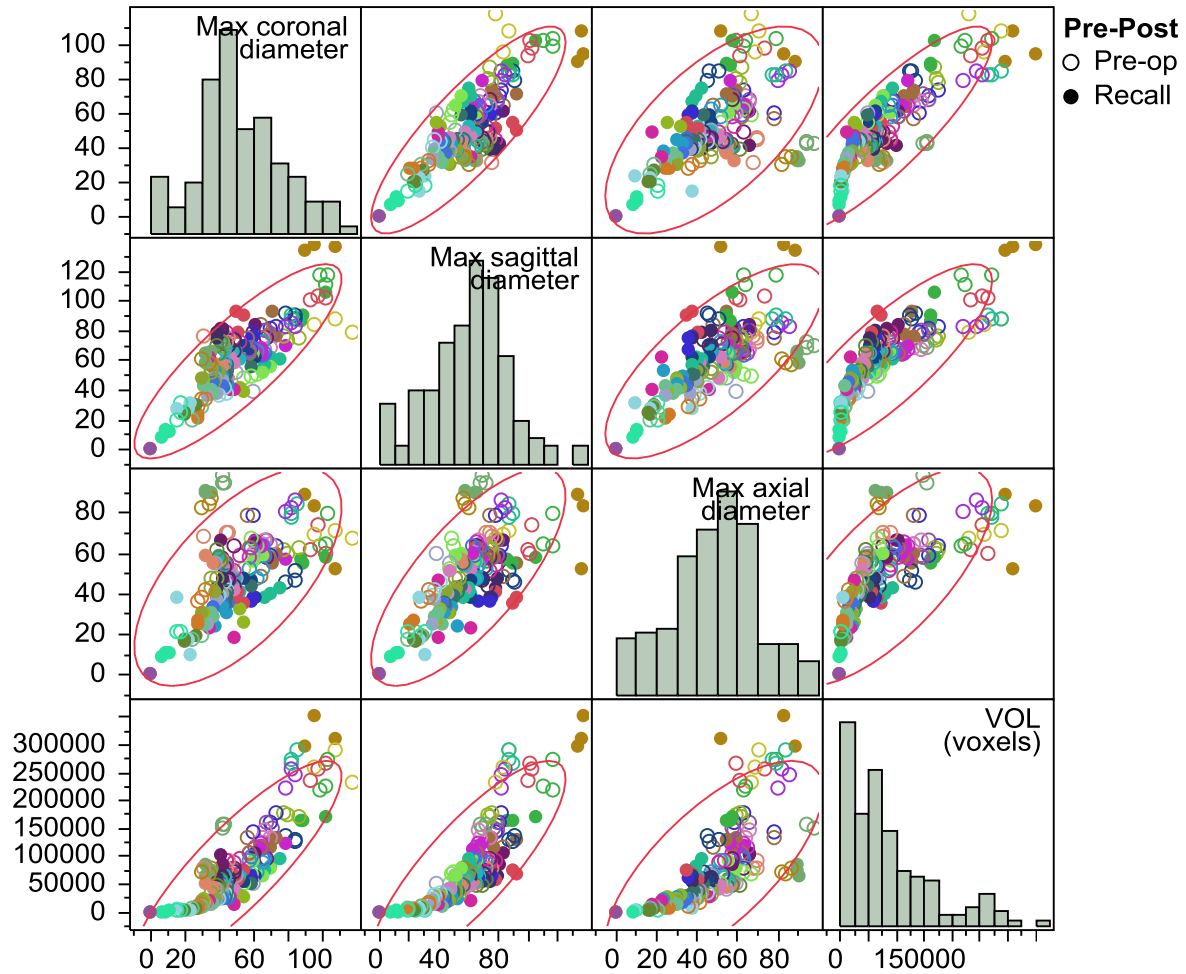
The measurements of volume by the DTG method resulted in a database with triplicate measurements for each person and occasion. Four variables were recorded: Max coronal diameter, Max sagittal diameter, Max axial diameter, and VOL (voxels). The units of these measurements is unknown. Table 7 shows the average, SD and range of values of each variable. The diameters are normally distributed but volume clearly is strong skewed (see Figure 11). One result of the skewed volume measurements is that the mean is strongly affected by the outliers; the mean (82,999) is much larger than the median (64,362).

Table 7. Descriptive Statistics for the DTG measurements

Variable	N	Mean	Std Dev	Minimum	Maximum
Max coronal diameter	180	50.611	24.663	0	118
Max sagittal diameter	180	59.561	26.703	0	138
Max axial diameter	180	48.333	21.908	0	98
VOL (voxels)	180	82998.922	77051.343	0	351422

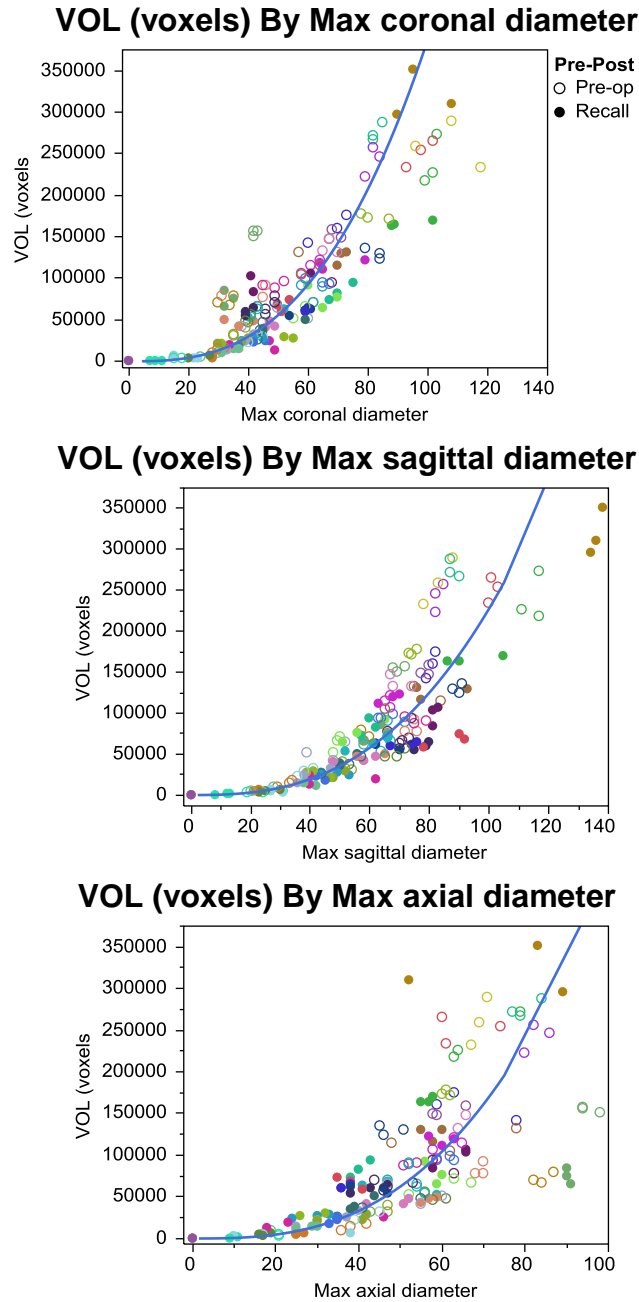
Variable	Correlations			
	Max coronal diameter	Max sagittal diameter	Max axial diameter	VOL (voxels)
Max coronal diameter	1	0.8472	0.6389	0.8573
Max sagittal diameter	0.8472	1	0.7472	0.8282
Max axial diameter	0.6389	0.7472	1	0.7137
VOL (voxels)	0.8573	0.8282	0.7137	1

Figure 11. Relationships Between the DTG measurements



There is a relationship between each of the diameters and volume (see Figure 12) but the relationship is not linear (not that it was expected to be). The curve in the figure is the result of fitting a straight line on the log scale of each variable. These figures illustrate that, whatever the DTG algorithm is doing, it is related to the diameters on each view.

Figure 12. Relationships Between the DTG Diameters and Volume

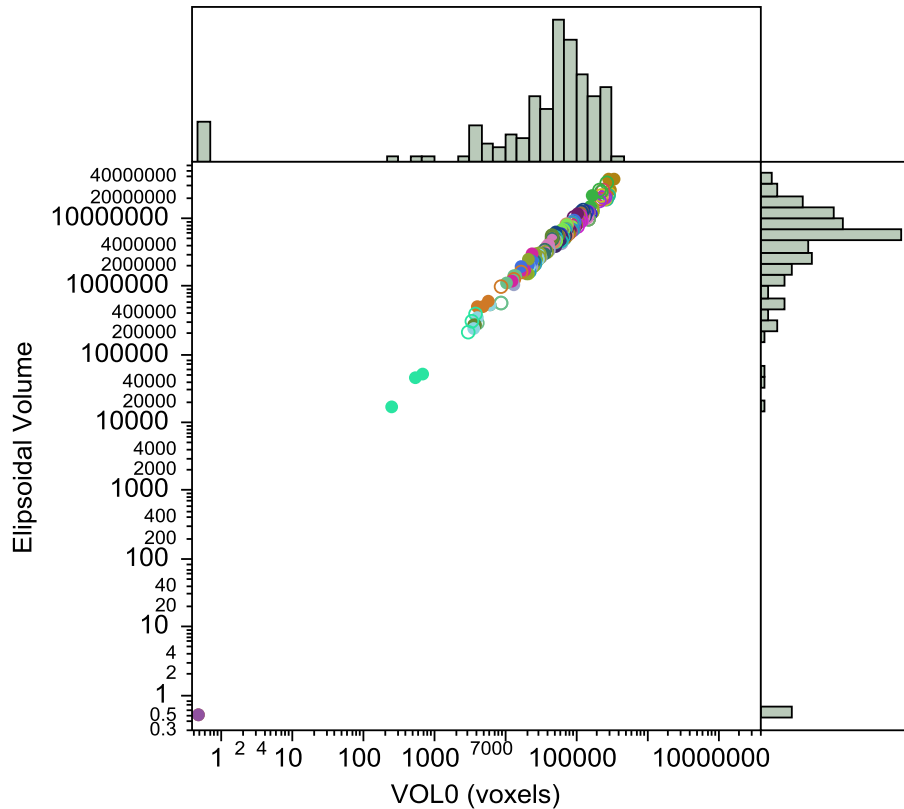


As an additional check, the volume of the lesion may be calculated from the three diameters. The volume of an ellipsoid with the principle axes (radii) of length a , b , and c is

Calculated Volume = $\frac{4}{3}\pi abc$. Using the max diameters as twice the radii in this formula, the volume may be calculated and compared to that obtained by DTG. Figure 13 shows that there is

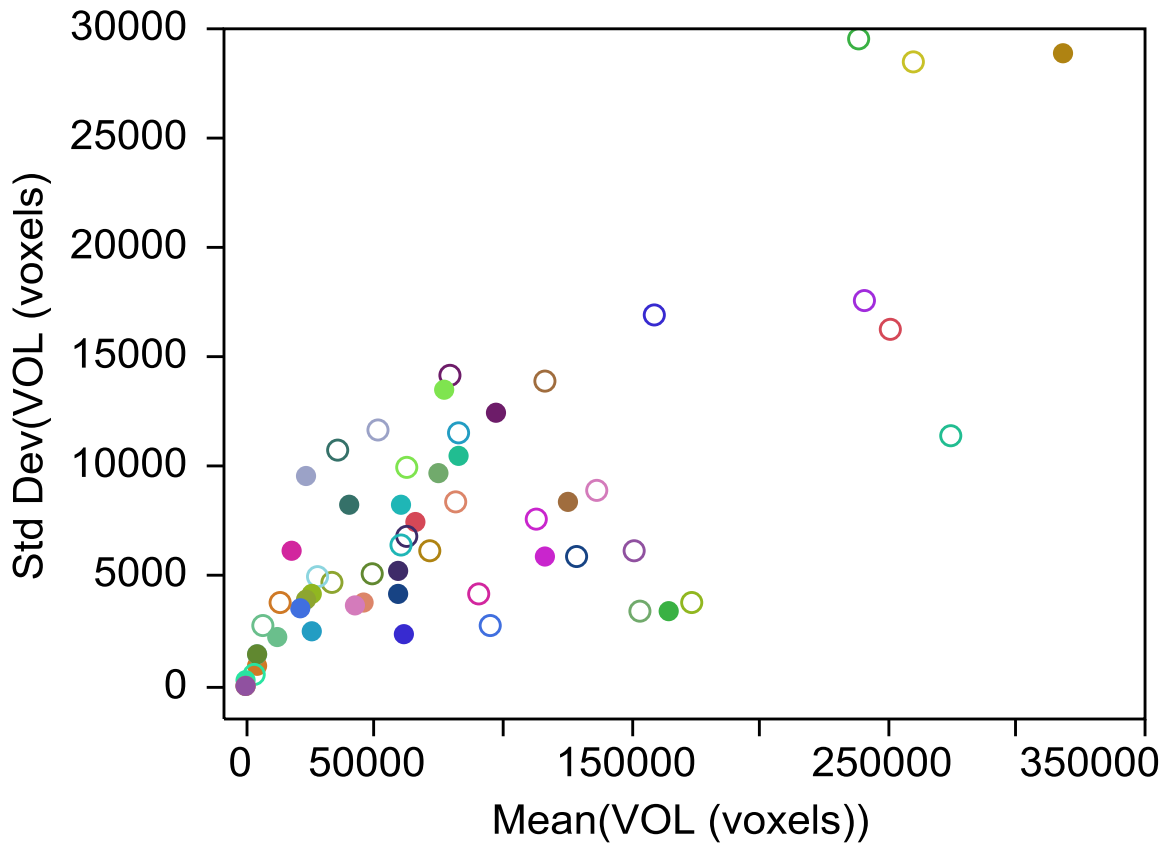
a near perfect correlation (Spearman's $\rho = 0.99$) but the scale is different. Note that the scatterplot is shown on the log scale but that poses a problem for the zero volume (as the log of zero is undefined). On this figure the zero volumes are shown as 0.5. The median DTG volume is 64,362 whereas the calculated volume is much larger (5,283,036).

Figure 13. Calculated Ellipsoidal Volume By VOL (voxels)



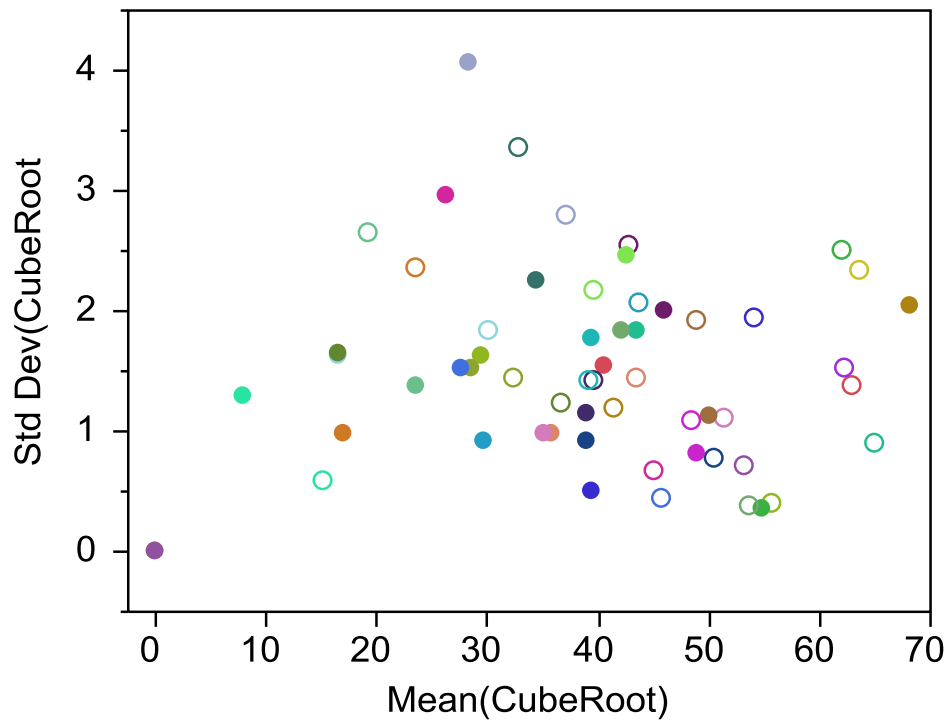
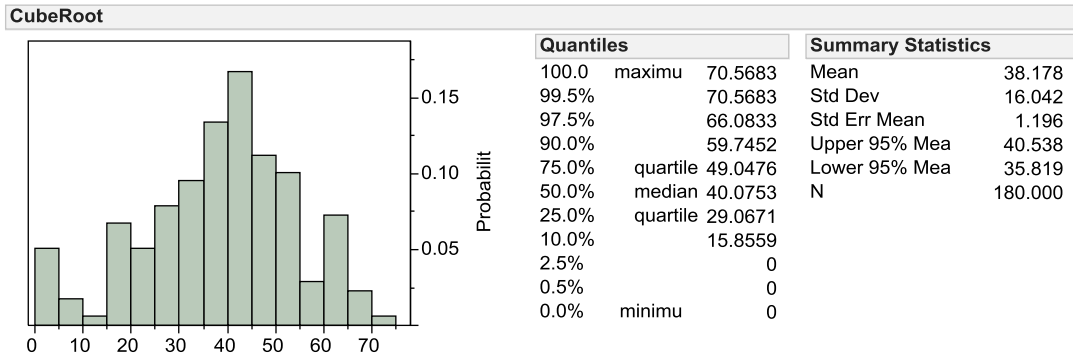
Which brings us to how to calculate the volume of each lesion using the triplicate measurement. Calculating a simple average will not do, since the measurement error clearly increases as the average increases—a direct result of the skewness. This may be seen in Figure 14 where it is apparent that as the mean volume increases, so too does the SD—it's much easier to measure a small volume.

Figure 14. Relationship Between the Mean and the SD



The solution is found through an understanding of the relationship between the diameters and volume. Clearly, volume has a cubic relationship to the diameters and so analyzing the cube-root of volume will remove the skewness and the SD of the cube-root measurements for each lesion is constant (Figure 15).

Figure 15. Cube Root of Volume



Discussion

Some questions have been raised regarding what constitutes a detectable periapical radiolucency. Estrella's group defined it as a lesion if the periodontal ligament space was wider than 0.5mm (65). However, Pope's 2014 study of teeth with a healthy periapex found that teeth with vital healthy pulp could have PDL space widening of 0-1mm (66). He also found two cases where healthy teeth demonstrated a periapical radiolucency of 2-4mm on CBCT scan. Pope concluded that the PDL space demonstrated significant variation when examined by CBCT. For the purposes of this study a PARL was defined as a radiolucency two times the width of the healthy periodontal ligament space present on an adjacent healthy tooth. This definition is consistent with studies done by van der Borden, Metska, Liang, and Zhang (61-64).

Several different methodologies have been employed in the evaluation of changes in the size of periapical radiolucencies using CBCT. Some studies have simply asked a yes or no question with regards to the presence of a radiolucency (67). Other studies have compared pre-operative and post-operative CBCT scans and classified the change in size of the lesion into categories (i.e. enlarged periapical radiolucency, unchanged periapical radiolucency, reduced periapical radiolucency) (68). Estrella developed a periapical index using CBCT based on Orstavik's similar index for radiographs (65, 69). Van der Borden's group was reportedly the first clinical study to use a volumetric analysis of periapical radiolucent lesions for the assessment of outcome (61).

Several in-vitro studies have confirmed the accuracy of CBCT in assessment of volumetric measurements for lesions. A 2007 study found volumetric measurements to be accurate when compared to multiple linear measurements of dry skull lesions in the human

maxilla (70). Alhowalia created artificial bone cavities to simulate periapical lesions and found that the volume could be accurately determined (59). Whyms reported similar findings (71).

DiThresh Gui volumetric software was developed by Anthony Fouad using MATLAB software. A pilot study was carried out at the University of Maryland to test the validity of the software (72). In the pilot, seven artificial bone lesions were created in a dry skull at the periapex of intact teeth. Two CBCT machines, Carestream Kodak 9000© and Planmeca Promax© were used to image the dry skulls. Using DiThreshGui software the volumes of each lesion was determined. Then impressions, using polyvinylsiloxane (PVS), were taken of each artificial bone lesion. A water displacement method was used to determine the volume of the PVS impression. The volume obtained by the water displacement method was compared with the volumes obtained by the software.

It was found that there was no significant difference in the volume measurement between the three groups (one-way ANOVA, $p < 0.05$). A positive correlation was found between the actual volumes and each of the CBCT machines (Kodak; $r = 0.5$, and Promax; $r = 0.45$). The pilot showed that the volumetric analysis using DTG provided an accurate representation of the true periapical lesion volume.

Periapical lesions often present as irregular three-dimensional shapes. Volumetric measurements should have an advantage over two-dimensional linear measurements because the irregularities of a given lesion can be measured and accounted for. However, in our personal experience, we found that obtaining accurate volumetric measurements can be challenging and time-consuming. It was quite simple to obtain reproducible, seemingly accurate volumetric measurements for well-defined lesions confined to trabecular bone. When lesions perforated through the cortical plate or into the maxillary sinus volumetric assessment was more difficult.

Since the relative radiodensity of the maxillary sinus or space outside of the cortical plate is approximately the same as periapical radiolucencies, it was often difficult to determine a clear boundary for perforating lesions. This resulted in difficulty obtaining reproducible measurements. DTG allows the user to observe a 3D model of the lesion after making the measurements. This 3D model was thoroughly examined to make sure that it reproduced the shape of the lesion as closely as possible. If the model did not accurately reproduce the shape then the measurement had to be re-done.

Volumetric measurements were also difficult to obtain if the CBCT scan quality was less than optimal. DTG software relies on the lesion being represented by radiolucent, dark colored pixels and the surround healthy bone to be represented by radiopaque, white colored pixels to make an accurate volumetric measurement. If the scan had scatter or radiographic artifacts the white/black contrast could be more difficult to assess. In addition to this, if the patient moved during scan acquisition, the white/black contrast could appear blurry and make determination of lesion boundaries, difficult or impossible.

It was interesting to note, in our study, that the linear measurements could be used to estimate a volume using an ellipsoid model that had a high degree of correlation with the volume obtained by DTG. This finding was considered to be significant because we found obtaining the linear measurements to be simpler and less time consuming when compared with the DTG measurements.

However, this is not to say, that obtaining linear measurements of periapical lesions was always a simple task. The radiologist observer had several instances where she did not feel confident in accurately assessing lesion boundaries. In these instances the radiologist did not record a measurement. The instances where this occurred can be found in Appendix E. We

accounted for this by not using the data where the radiologist did not record a linear measurement in our statistical calculation.

Our results showed differences in how the radiologist and endodontist interpreted lesion size. Multiple factors, including scan quality, size of the lesion, as well as background, training, and experience may influence CBCT interpretation. Classic endodontic studies have shown that bias can be present when radiographs are interpreted (27, 73). In our study we found that interpreter bias exists when CBCTs are interpreted as well.

A periapical radiolucency may represent one of several different types of lesions. Most agree that treatment options for the different lesions of apical periodontitis are the same, either extraction or nonsurgical root canal therapy. However, several authors have disagreed. Most of the controversy has involved treatment of teeth with periapical cysts.

Simon (74) was the first to describe two different types of apical cysts. He described cysts completely enclosed by epithelial lining as *true cysts* and those that had epithelial lining that was in direct connection with the root canal lumen as *bay cysts*. Nair (9) suggested the term *pocket cysts* to replace *bay cysts*. Without any supporting experimental data some have suggested that *pocket cysts* may heal following nonsurgical root canal treatment, while *true cysts* may not be capable of doing so (75).

It is important to note that while some authors have suggested that healing of apical cysts may not be possible following nonsurgical root canal therapy (75), others have suggested that it is not only possible but probable following reduction of the microbial load within the root canal space (76). Lin suggested a mechanism for regression of apical cysts following nonsurgical root canal therapy (76). He suggested that the epithelial cells that line the cystic cavity may be forced to undergo apoptosis as the newly formed bone reaches the vicinity of the cyst. As the epithelial

cells apoptose a fibrous connective tissue may be capable of penetration of the cystic cavity and serve as a scaffold for subsequent healing of the lesion.

Most studies have shown that differentiation between a periapical cyst and periapical granuloma cannot be done using radiographs alone (77). Some studies have provided evidence that interpretation of lesions on CBCT may provide a more accurate diagnosis between cysts and granulomas (78, 79). However, another study found that CBCT was not a reliable diagnostic tool for differentiation of periapical cysts from granulomas (80). Surgical biopsy and histopathologic evaluation remain the gold standard for identification of periapical lesions. In this study no attempt was made to try to differentiate between periapical cysts and periapical granulomas. It is plausible that the healing dynamics of periapical cysts differ from periapical granulomas differ, however, this has not been definitively shown.

Healing of periapical lesions has been reported to occur by fibrous scar tissue occasionally, which is not distinguishable radiographically from an apical granuloma (81, 82). However, the best available data suggests that healing by scar tissue rarely occurs, perhaps 1-2% of the time or less (83, 84). Therefore, it seems that in most cases periapical radiolucencies associated with teeth represent pathological lesions and not scar tissue. In this study no attempt was made to determine if the periapical radiolucency present with endodontically treated teeth was fibrous scar tissue. The only accurate way to determine this is by surgical biopsy.

Several recent studies have concluded that a significant number of teeth diagnosed as healthy following endodontic treatment, based upon periapical radiographs, show evidence of periapical radiolucency on CBCT scans (39, 85). Multiple studies have shown that CBCT is capable of detecting small lesions not observable on radiographs (36, 38). This fact has led some to suggest that CBCT may overestimate the frequency of periapical lesions (86). Some have

raised questions about if treating all asymptomatic lesions will lead to overtreatment. However, a histological study by Love & Firth found that out of 100 periapical lesions, submitted for biopsy following endodontic surgery, only 2% were scars, the other 98% were either periapical granulomas or cysts (83). Schultz had similar findings, out of 125 samples 98% of periapical radiolucencies were confirmed as inflammatory periapical lesions (cysts, granulomas, or abscesses). Therefore, it is reasonable to assume that the vast majority of periapical radiolucencies represent pathological lesions of an inflammatory nature.

Although Orstavik's classic radiographic study found that the peak incidence of healing was at one year, CBCT studies have found relatively low rates of complete healing one year after treatment (22). Patel found complete resolution of 48% of lesions at one year but Liang and van der Borden found only 19% and 16% respectively (61, 64, 68). Importantly, Zhang found that 22% of lesions that were not completely healed one year after treatment were completely healed at the two-year follow up (62). Van der Borden and others have suggested that assessment of healing of apical periodontitis using CBCT vs PA radiographs may be different.

Our study found that the only instances where periapical lesions showed complete resolution were at 10 months or more following the initiation of treatment. This is consistent with Orstavik's finding that the peak incidence of healing is at one year following treatment (22). The low incidence of complete resolution, 3 out of 30 lesions, is consistent with findings by van der Borden, Liang, and Zhang, and likely attributable to the fact that post-operative CBCTs were taken at one year or less (61, 62, 64).

There is some inconsistency in the literature regarding the timeline of healing of apical periodontitis. Two studies by Molven have shown that lesions persistent beyond 4 years following treatment may heal more than 17 years after endodontic treatment (87, 88). In our

study several of the lesions, 5 out of 30, did not change in size. Molven's study suggests that these lesions still have the potential to decrease over time. Well-controlled, long-term studies are needed to better elucidate the timeline of healing of apical periodontitis.

Healing is dynamic and it is affected by many factors. There are many factors that may affect healing of apical periodontitis including systemic health and age that were not evaluated in this study. Therefore, the results from this study may not be applicable to studies that control for these types of factors.

CBCT will allow for the healing of periapical lesions following endodontic treatment to be studied in a way that was not possible using PA radiographs. For example, future studies can focus, not only, on the timeline for healing of periapical lesions but also on lesions with different characteristics. Using CBCT healing could be studied for lesions that are confined solely to cancellous bone. Healing could be studied for lesions perforating through one cortical plate, or both cortical plates (through and through). Specific timelines for re-establishment of the cortical plate(s) could be determined using CBCT. Likewise timelines could be studied for lesions perforating through into maxillary sinus or extending into intraradicular (furcal) bone.

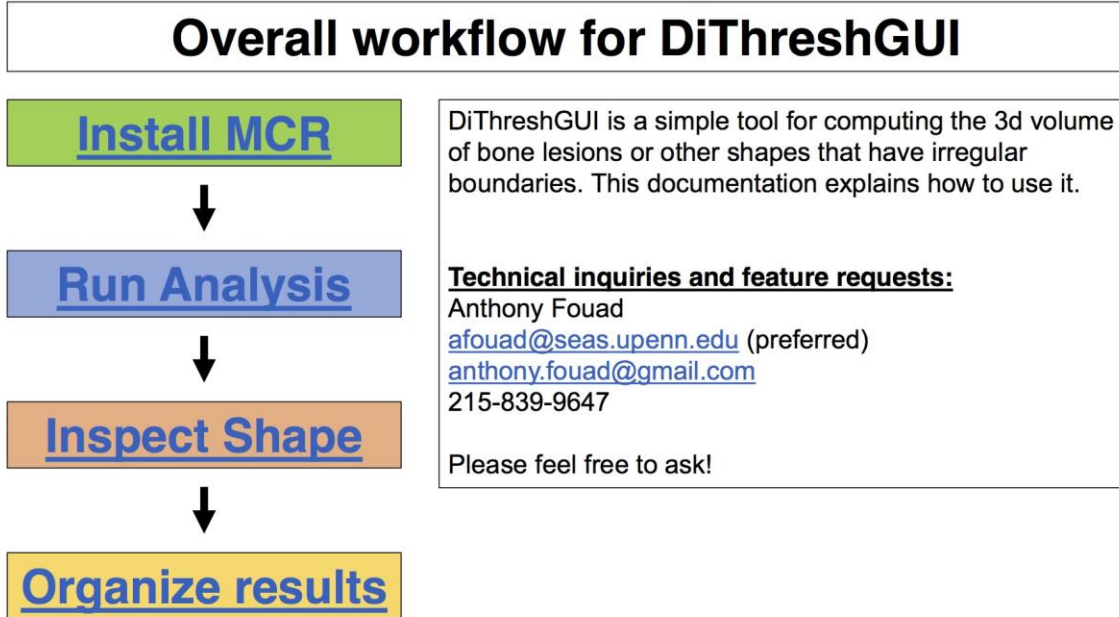
It would also be interesting in the future to compare CBCT to PA radiographs to see if healing can be detected at earlier points in time using CBCT. In addition to this, work could establish how often an early decrease in the size of a PARL predicts complete resolution of a lesion in the future. If it was demonstrated that early healing was predictive of complete resolution of a lesion, then future clinical trials could potentially assess healing at much earlier points in time than they currently can with PA radiography alone.

In conclusion, we found that a change in the size of periapical radiolucencies can be detected 3-12 months post non-surgical endodontic treatment. A decrease in the size of periapical

radiolucencies can be detected as early as 91 days following the initiation of treatment. Additionally, it was found that there is a near-perfect correlation (Spearman's rho = 0.99) between calculated volume from three diameters and volumetric software when calculating lesion volume.

Appendix A

Protocol for DiThreshGui Volumetric Measurements



[Back to main](#)

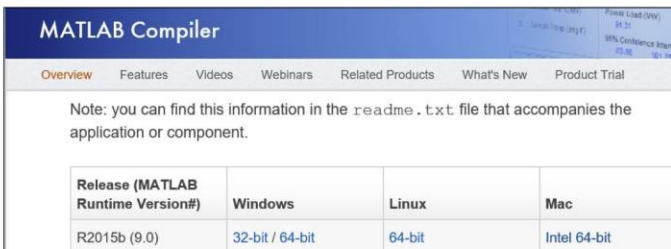
Install MCR

1 of 1

DiThreshGUI_2015b requires that you download and install the **Matlab Compiler Runtime R2015b**. MCR is available here:

<http://www.mathworks.com/products/compiler/mcr/index.html>

MCR is **free** and does not require a Matlab License.
Please select the version that matches your computer system.



Release (MATLAB Runtime Version#)	Windows	Linux	Mac
R2015b (9.0)	32-bit / 64-bit	64-bit	Intel 64-bit

Alternately, the DTG source code can be run from within Matlab.

[Back to main](#)

Run analysis

1. Double click on **DiThreshGUI_2015b**.
2. Click **XY Dicom** to load a stack of dicom images*,**.
3. In the popup window, navigate to your DICOM images. Select **ALL** of them, and press **open**.

* DiThreshGUI will offer to save the 3D stack after it puts together all slices. This stack can be used instead of the dicoms if you click **XYZ mat** next time you run the program.

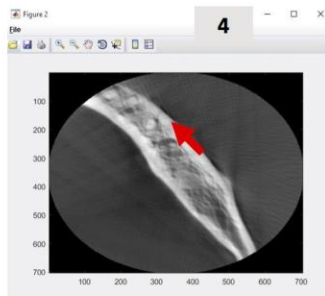
** All button in DiThreshGUI turn **Red** while they are processing and **Green** when they are done. If a button remains red, it has crashed and you will not be able to continue your analysis. Please contact Anthony.

[Back to main](#)

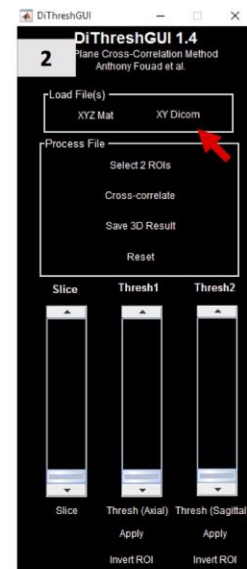
Run analysis

4. The **Slice** slider bar turns **Yellow**. This indicates it is ready to be used next.

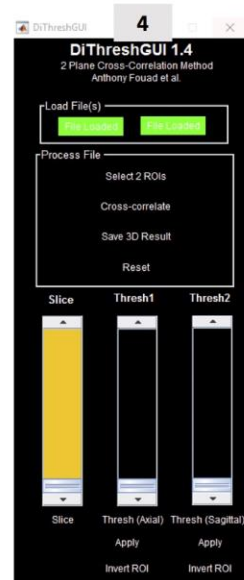
Navigate through the axial slices until you find the lesion. When ready, click **Select 2 ROIs**.



1 of 8



2 of 8



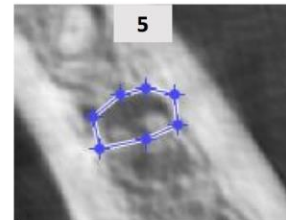
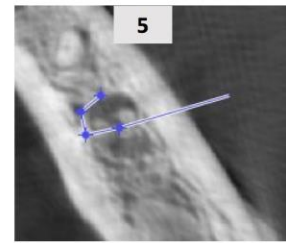
[Back to main](#)

Run analysis

5. Use the polygon tool to draw a subjective boundary around the lesion in the axial plane:
 - Click to add a new point
 - Click on the first point to close the shape.
 - **OR**, double click to force close the shape.
 - When finished, **double click** in the center of the shape to exit.

The boundary need not be precise. It is refined by thresholding later. When you preview your 3D results later, you will be able to tell whether the boundary you drew was suitable.

3 of 8



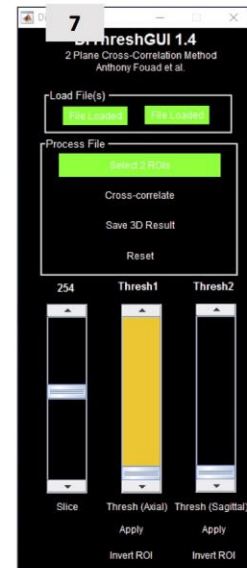
[Back to main](#)

Run analysis

6. A new pop up shows a sagittal slice that passes through the shape you drew in step 5. Again, draw a boundary around your lesion in the sagittal plane. Again, double click to complete*.
7. After a few seconds, Select 2 ROIs turns **Green** to indicate completion and the **Thresh1** slider turns **Yellow**, advising you to use it next.

* DiThreshGUI may crash if the boundary you draw in the sagittal plane does not intersect the boundary you drew in the axial plane. DTG does not currently check for this error – it relies on the user to select the same lesion in both views.

4 of 8

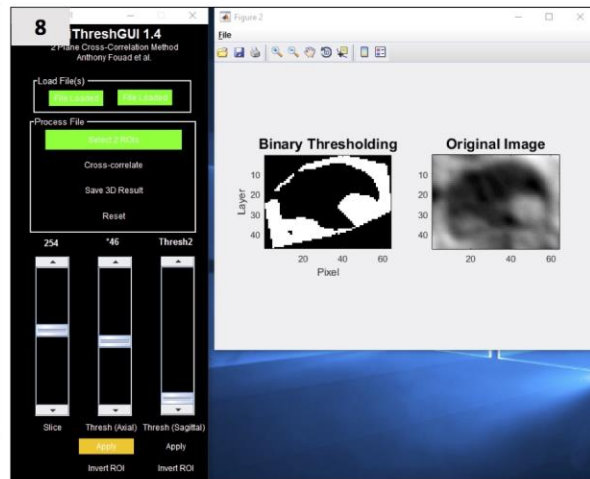


[Back to main](#)

Run analysis

5 of 8

8. Use the **Thresh1** slider to select an appropriate threshold for the lesion*.
9. When satisfied, click **Apply** and then **Invert ROI**.
10. Now, Repeat 6 and 7 with **Thresh2** in the sagittal plane.



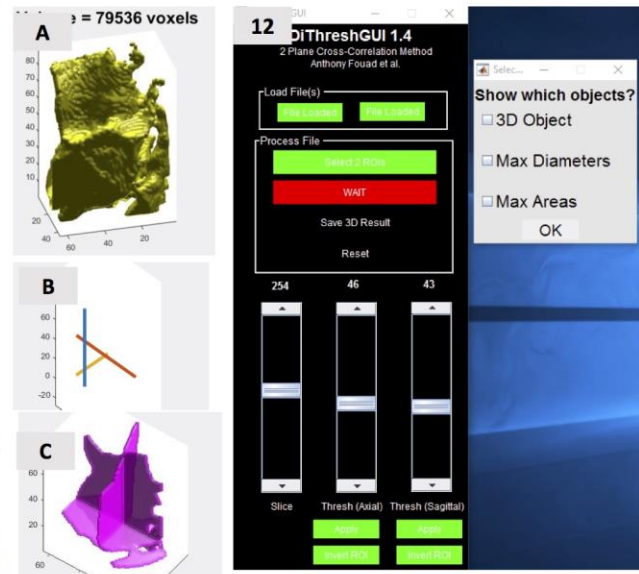
* If needed, you may record the specific threshold and use the same one later (46 in this case)

[Back to main](#)

Run analysis

6 of 8

11. When both thresholds are set, the **Cross-Correlate** button turns **Yellow**, advising you to click it.
12. In the popup window, you can select from 3 display options. Click any combination of these and press **OK****.
 - A – 3D object
 - B – Max Diameters
 - C – Max Areas



* You can click Cross-Correlate again to try a different graphical representation.

** The rotation tool on the pop up window is useful for adjusting the 3D object's orientation.

[Back to main](#)

Run analysis

7 of 8

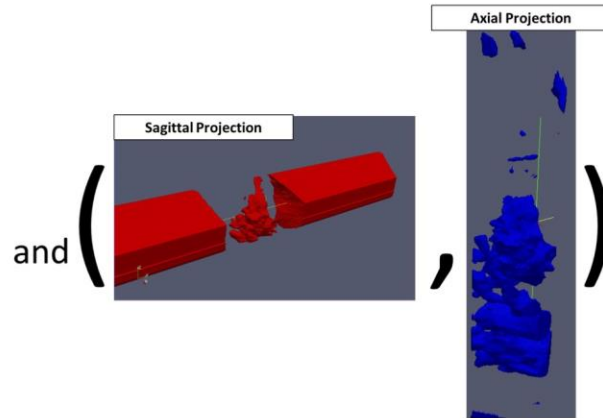
How does this work?

The axial threshold you selected is applied to all frames in the axial direction (blue object at right).

The sagittal threshold you selected is applied to all slices in the sagittal direction.

The intersection of these two objects is the lesion.

This algorithm is substantially similar to **Metska et al (2013), JOE, Volumetric Changes in Apical...**, but was developed independently and does not require AMIRA.



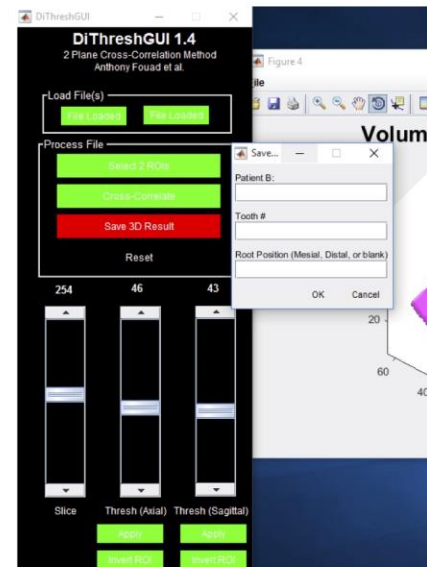
[Back to main](#)

Run analysis

8 of 8

13. Regardless of which 3D view you choose to preview, you can click **Save 3D result** to save all of the information to disk. Type in the patient ID (B#), Tooth #, and Root position (e.g. Mesial) and click **OK**.

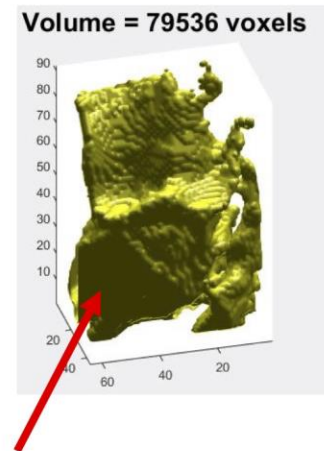
14. A .mat file containing all of this information is saved to the same directory as the 3D image you loaded. You can convert this file to an excel file using the **Organize Results** section later.



[Back to main](#)

Inspect shape

- Be sure that the 3D shape faithfully represents what you consider to be lesion. In particular, large flat faces (**arrow**) indicate that your shape was cut off by the region(s) of interest you drew. If this is not desired, you can try again with a larger ROI by pressing the **Reset** button.
- In general, the region selection strategy and threshold levels will substantially impact the resulting shape and its reported volume. You should be careful to standardize the thresholds used and train the user on training data before evaluating experimental subjects.



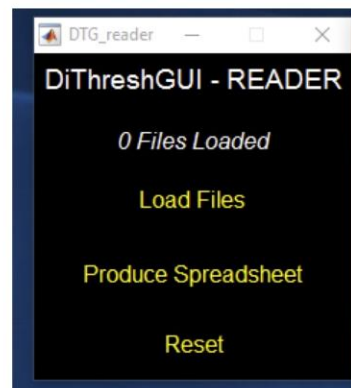
1 of 1

[Back to main](#)

Organize Results

- After completing several 3D analyses, you will have a collection of files with format:

DTG_B#_tooth#pos.mat
- These files can be collected together into an excel spreadsheet that contains volumetric, diameter and area information using the separate standalone **DTG_reader_2015b**
- Run this application by double clicking on it.
- Click on **Load Files**, and then select ALL of the DiThreshGUI output results you would like to organize.



1 of 2

Organize Results

2 of 2

- Click produce spreadsheet when you have all of them. Type a filename.
- A popup tells you where the xlsx was saved (same directory where DTG_reader_2015b is located). This file contains all of the volume, diameter and area information for each file you processed.

	A	B	C	D	E	F	G	H	I	J
1	Measurement:	B01	B05	B07	B07	B07	B77	B88	B88	B12
2	Date of processing	3-Jun-13	22-Sep-15	6-May-13	6-May-13	6-May-13	14-Jul-14	22-Jun-14	22-Jun-14	22-Sep-15
3	Time of processing	09:07.3	18:18.6	48:08.8	50:20.5	43:01.5	37:43.0	16:36.0	27:25.6	21:20.7
4	Axial Threshold	0.61	0.39	0.37	0.37	0.37	0.34	0.4	0.4	0.46
5	Sagittal Threshold	0.61	0.4	0.36	0.36	0.36	0.34	0.41	0.4	0.43
6	Coordinates of lesion (R,C,F):	397,366,403	250,334,241	473,419,280	380,389,273	249,330,252	128,216,285	252,339,234	248,331,234	251,328,254
7	VOL (voxels):	58908	61123	30151	11863	50003	20012	108481	73801	79536
8	Max coronal diameter:	61	33	37	22	30	27	45	35	34
9	Max coronal area:	2084	2678	1089	795	2324	1035	3272	3028	3186
10	Max sagittal diameter:	44	53	46	46	50	37	68	63	64
11	Max sagittal area:	2387	1583	894	392	1363	882	2110	1705	1866
12	Max axial diameter:	64	70	40	32	67	41	79	72	76
13	Max axial area:	1495	1355	1396	564	1190	620	2068	1609	1577
14										

Appendix B

Protocol for Lesion Measurement

1. Identify the tooth and specific root(s) associated with the lesion in question
2. View the scan using orthogonal slicing
3. View the scan in 1.2-1.3mm slice thickness

Do the following for the Axial, Coronal, and Sagittal Planes

4. Scan through the entire plane and identify the slice where you feel the lesion has the largest overall area
5. Make a measurement across the lesion (from bone to bone) that represents the largest diameter, or largest measurement of the lesion (note that this measurement can be in any direction across the lesion)*
6. Next, make a measurement at 90 degrees to the initial measurement
7. Record these two measurements
8. Perform these measurements on both the pre-op & post-op views, then record your assessment of the change in lesion size over time using the 3 point modified Likert scale provided

*If the lesion does not have clear bone boundaries (i.e. cortical plate perforation, sinus perforation etc.), then estimate the lesion boundary based upon the bone that can be observed on either side of the defect

Appendix C

Identifier	Date CBCT was taken	Endo Tx	Root (if applicable)	Tx Initiated	Tx Completed	# Endo Appts	Pt Age	Interappointment CBCT
B1, B2	7/30/14	#31 NSReTx		8/20/14	9/9/14	3	63	No
C1, C2	8/14/14	#15 NSReTx		8/26/14	10/6/14	4	61	No
D1, D2	3/18/15	#19 NSReTx		3/25/15	4/8/15	3	37	No
E1, E2	11/5/14	#8 NSRCT		11/5/14	11/25/14	2	72	No
F1, F2	2/20/15	#7 NSRCT		4/2/15	5/4/15	2	21	No
G1, G2	2/20/15	#8 NSRCT		4/2/15	5/4/15	2	21	No
H1, H2	2/20/15	#9 NSRCT		4/2/15	5/4/15	2	21	No
I1, I2	3/17/15	#3 NSRCT	MB	4/1/15	4/29/15	2	38	No
J1, J2	3/17/15	#3 NSRCT	P	4/1/15	4/29/15	2	38	No
K1, K2	3/17/15	#4 NSRCT		4/1/15	4/29/15	2	38	No
L1, L2	11/4/14	#30 NSReTx		11/4/14	12/1/14	3	48	No
M1, M2	10/27/14	#12 NSReTx		10/27/14	11/3/14	2	45	No
N1, N2	9/3/14	#12 NSRCT		8/20/14	9/17/14	3	78	Yes
O1, O2	6/9/15	#3 NSReTx	MB	5/21/15	6/9/15	2	48	Yes
P1, P2	6/9/15	#3 NSReTx	P	5/21/15	6/9/15	2	48	Yes
Q1, Q2	6/19/15	#30 NSReTx	M	6/22/15	7/9/15	3	67	No
R1, R2	6/19/15	#30 NSReTx	D	6/22/15	7/9/15	3	67	No
S1, S2	12/5/14	#5 NSRCT	B	11/25/14	3/16/15	4	70	Yes
T1, T2	12/5/14	#5 NSRCT	P	11/25/14	3/16/15	4	70	Yes
U1, U2	6/30/15	#3 NSRCT		6/30/15	7/15/15	2	63	No
V1, V2	8/28/14	#19 NSReTx		9/29/14	10/21/14	2	28	No
W1, W2	2/19/15	#14 NSReTx		2/6/15	2/19/15	2	71	Yes
X1, X2	1/9/15	#30 NSRCT	M	11/26/14	2/9/15	4	67	Yes
Y1, Y2	1/9/15	#30 NSRCT	D	11/26/14	2/9/15	4	67	Yes
Z1, Z2	5/29/15	#30 NSReTx		5/29/15	6/11/15	2	54	No
AA1, AA2	7/9/15	#21 NSRCT		7/9/15	7/29/15	2	23	No
AB1, AB2	7/21/15	#14 NSReTx		8/6/15	8/25/15	2	39	No
AC1, AC2	8/19/15	#14 NSRCT	MB	8/19/15	9/9/15	2	21	No
AD1, AD2	8/19/15	#14 NSRCT	DB	8/19/15	9/9/15	2	21	No
AE1, AE2	8/19/15	#14 NSRCT	P	8/19/15	9/9/15	2	21	No

Identifier	Days b/t CBCT and Initiation of Tx (mo)	Days b/t initiation of Tx and Completion of Tx	Date of Post-Op CBCT	Days b/t initiation of tx and post op CBCT
B1, B2	21	20	42226	355
C1, C2	12	41	42233	356
D1, D2	7	14	42234	146
E1, E2	0	20	42247	299
F1, F2	41	32	42247	151
G1, G2	41	32	42247	151
H1, H2	41	32	42247	151
I1, I2	15	28	42248	153
J1, J2	15	28	42248	153
K1, K2	15	28	42248	153
L1, L2	0	27	42250	303
M1, M2	0	7	42261	322
N1, N2	-14	28	42261	390
O1, O2	-19	19	42264	119
P1, P2	-19	19	42264	119
Q1, Q2	3	17	42275	98
R1, R2	3	17	42275	98
S1, S2	-10	111	42275	307
T1, T2	-10	111	42275	307
U1, U2	0	15	42276	91
V1, V2	32	22	42278	367
W1, W2	-13	13	42282	241
X1, X2	-44	75	42284	315
Y1, Y2	-44	75	42284	315
Z1, Z2	0	13	42289	136
AA1, AA2	0	20	42291	97
AB1, AB2	16	19	42313	91
AC1, AC2	0	21	42331	96
AD1, AD2	0	21	42331	96
AE1, AE2	0	21	42331	96

Appendix D

DiThreshGui Results

Lesion Identifier	Axial Threshold	Sagittal Threshold	VOL (voxels)	Max coronal diameter	Max sagittal diameter	Max axial diameter
B1	0.33	0.42	222178	79	82	80
B1	0.37	0.38	245903	84	82	86
B1	0.43	0.39	256466	82	85	82
B2	N/A	N/A	0	0	0	0
B2	N/A	N/A	0	0	0	0
B2	N/A	N/A	0	0	0	0
C1	0.29	0.26	258214	96	83	69
C1	0.24	0.26	232406	118	78	67
C1	0.24	0.25	289207	108	88	71
C2	N/A	N/A	0	0	0	0
C2	N/A	N/A	0	0	0	0
C2	N/A	N/A	0	0	0	0
D1	0.27	0.28	65556	43	67	54
D1	0.26	0.29	53137	41	64	56
D1	0.31	0.27	61900	43	58	54
D2	0.20	0.23	52433	40	52	59
D2	0.23	0.20	68618	50	66	47
D2	0.24	0.25	62553	52	61	41
E1	0.45	0.44	114279	61	65	65
E1	0.45	0.46	121118	64	67	63
E1	0.43	0.45	105913	58	67	58
E2	0.46	0.43	122007	79	70	57
E2	0.50	0.48	118769	64	68	63
E2	0.46	0.48	110650	65	63	60
F1	0.37	0.39	170683	87	74	62
F1	0.43	0.45	172643	80	73	60
F1	0.40	0.40	177855	78	76	61
F2	0.20	0.27	26728	55	39	26
F2	0.22	0.29	29482	52	41	32
F2	0.24	0.28	21260	31	47	30
G1	0.39	0.40	89316	65	72	52
G1	0.40	0.40	70294	62	66	47
G1	0.43	0.43	90820	58	66	52
G2	0.23	0.28	27195	45	44	30
G2	0.22	0.25	27874	42	49	33
G2	0.25	0.31	23423	38	53	24
H1	0.45	0.45	95794	52	72	59
H1	0.47	0.43	87657	49	75	51
H1	0.44	0.44	90916	45	79	54
H2	0.29	0.34	24594	47	40	46
H2	0.28	0.30	12484	49	40	18
H2	0.43	0.34	18954	34	62	23
I1	0.57	0.54	30802	35	54	47
I1	0.53	0.48	31901	35	52	43
I1	0.52	0.46	39301	39	51	47
I2	0.50	0.48	28023	40	52	42
I2	0.50	0.33	20899	30	48	30
I2	0.54	0.44	21860	38	45	41
J1	0.56	0.47	8803	30	28	19
J1	0.55	0.47	9075	30	28	19
J1	0.51	0.43	4237	24	20	17
J2	0.48	0.41	10468	31	42	25
J2	0.46	0.49	14460	37	38	29
J2	0.47	0.47	14005	35	40	30

Lesion Identifier	Axial Threshold	Sagittal Threshold	VOL (voxels)	Max coronal diameter	Max sagittal diameter	Max axial diameter
K1	0.26	0.37	135593	79	91	45
K1	0.27	0.48	123771	84	90	46
K1	0.28	0.51	129658	84	88	51
K2	0.21	0.26	62388	61	62	38
K2	0.21	0.27	60493	59	62	46
K2	0.23	0.32	54518	54	70	47
L1	0.43	0.42	158473	68	80	66
L1	0.44	0.44	147110	67	80	59
L1	0.43	0.42	149111	71	77	58
L2	N/A	N/A	0	0	0	0
L2	N/A	N/A	0	0	0	0
L2	N/A	N/A	0	0	0	0
M1	0.21	0.20	76918	45	72	70
M1	0.21	0.22	91619	46	75	70
M1	0.22	0.19	77639	31	76	68
M2	0.22	0.20	47253	42	56	57
M2	0.20	0.20	42126	37	58	55
M2	0.32	0.22	49407	32	65	59
N1	0.44	0.41	47218	39	69	61
N1	0.45	0.42	46322	40	65	58
N1	0.46	0.50	55453	41	72	56
N2	0.42	0.43	3979	20	25	16
N2	0.43	0.44	3625	20	23	17
N2	0.47	0.47	6266	27	30	19
O1	0.47	0.42	3439	18	24	21
O1	0.45	0.40	3100	15	19	21
O1	0.47	0.42	3904	18	31	21
O2	0.13	0.24	262	7	8	9
O2	0.15	0.25	542	9	13	11
O2	0.16	0.25	711	11	12	11
P1	0.39	0.49	51041	60	39	60
P1	0.40	0.40	41101	38	48	55
P1	0.43	0.42	64387	50	52	47
P2	0.37	0.29	32432	42	47	40
P2	0.34	0.32	24547	39	38	37
P2	0.37	0.41	13586	33	36	25
Q1	0.50	0.41	77554	49	66	63
Q1	0.56	0.42	94243	68	74	58
Q1	0.44	0.46	66227	43	71	53
Q2	0.36	0.36	106212	61	83	66
Q2	0.53	0.51	102899	41	81	66
Q2	0.55	0.49	83306	42	81	58
R1	0.46	0.42	104304	58	65	62
R1	0.52	0.45	114418	64	84	48
R1	0.46	0.43	131618	57	75	78
R2	0.49	0.39	129661	71	93	55
R2	0.29	0.36	115682	70	77	58
R2	0.30	0.36	130581	73	76	60
S1	0.20	0.23	70674	62	50	63
S1	0.20	0.26	66051	59	49	67
S1	0.18	0.20	51552	55	48	52
S2	0.17	0.15	64754	65	51	59
S2	0.17	0.19	76398	70	56	60
S2	0.20	0.15	91592	60	65	56

Lesion Identifier	Axial Threshold	Sagittal Threshold	VOL (voxels)	Max coronal diameter	Max sagittal diameter	Max axial diameter
T1	0.19	0.22	36825	44	53	41
T1	0.19	0.21	46860	45	57	55
T1	0.17	0.24	25392	43	44	35
T2	0.17	0.17	50104	59	56	44
T2	0.17	0.18	37867	45	50	39
T2	0.16	0.19	34493	45	50	38
U1	0.28	0.26	160186	70	81	59
U1	0.27	0.26	175115	73	82	63
U1	0.29	0.36	141382	60	79	78
U2	0.17	0.19	64337	60	76	38
U2	0.17	0.20	60778	59	74	36
U2	0.18	0.25	59924	59	67	36
V1	0.49	0.48	131533	70	68	64
V1	0.48	0.47	131783	65	74	64
V1	0.51	0.51	146924	67	67	66
V2	0.47	0.43	40325	46	48	51
V2	0.40	0.45	47239	47	62	52
V2	0.39	0.40	41627	49	58	42
W1	0.22	0.24	70257	30	60	82
W1	0.26	0.27	78438	35	57	87
W1	0.23	0.26	66393	34	58	84
W2	0.19	0.22	296074	90	134	89
W2	0.19	0.19	351422	95	138	83
W2	0.20	0.18	309517	108	136	52
X1	0.38	0.34	156723	42	72	94
X1	0.41	0.36	155686	43	68	94
X1	0.35	0.40	150540	42	69	98
X2	0.17	0.17	84607	32	64	90
X2	0.18	0.14	65173	32	58	91
X2	0.18	0.13	75065	35	66	90
Y1	0.44	0.45	28939	45	38	42
Y1	0.45	0.44	31902	43	41	45
Y1	0.43	0.47	22339	40	36	39
Y2	0.23	0.19	6250	15	27	38
Y2	0.27	0.33	3613	23	31	10
Y2	0.28	0.34	4053	22	27	17
Z1	0.22	0.35	62157	46	70	47
Z1	0.24	0.26	69930	49	73	44
Z1	0.23	0.22	56436	46	70	46
Z2	0.31	0.30	59430	39	79	43
Z2	0.32	0.30	64418	42	80	47
Z2	0.29	0.29	54019	39	75	38
AA1	0.48	0.47	233590	93	100	61
AA1	0.50	0.49	265694	102	101	60
AA1	0.52	0.46	254311	98	103	74
AA2	0.54	0.55	58519	51	78	41
AA2	0.57	0.51	67342	50	92	38
AA2	0.53	0.53	73400	54	90	35
AB1	0.26	0.46	272403	103	117	79
AB1	0.27	0.38	217461	99	117	63
AB1	0.28	0.37	226222	102	111	64
AB2	0.26	0.36	169383	102	105	58
AB2	0.24	0.36	163605	88	86	57
AB2	0.24	0.27	163696	89	90	55

Lesion Identifier	Axial Threshold	Sagittal Threshold	VOL (voxels)	Max coronal diameter	Max sagittal diameter	Max axial diameter
AC1	0.13	0.13	93417	67	64	59
AC1	0.15	0.14	94187	65	63	63
AC1	0.15	0.15	98428	59	68	62
AC2	0.13	0.12	17665	37	45	33
AC2	0.12	0.13	24452	46	42	35
AC2	0.12	0.14	22233	42	42	35
AD1	0.15	0.16	16822	32	34	42
AD1	0.13	0.14	9256	28	29	36
AD1	0.14	0.14	13779	30	33	38
AD2	0.14	0.14	5862	28	23	27
AD2	0.13	0.14	4969	28	21	25
AD2	0.13	0.14	4148	28	21	25
AE1	0.14	0.16	271124	82	87	77
AE1	0.14	0.14	288024	85	87	84
AE1	0.15	0.14	266545	82	90	79
AE2	0.11	0.13	72953	67	57	38
AE2	0.12	0.12	93796	75	60	43
AE2	0.12	0.12	81614	70	62	40

Sample	Mean VOL (Voxels)	Standard Deviation
B1	241516	17560
B2	0	0
C1	259942	28440
C2	0	0
D1	60198	6382
D2	61201	8177
E1	113770	7615
E2	117142	5851
F1	173727	3707
F2	25823	4185
G1	83477	11441
G2	26164	2398
H1	91456	4095
H2	18677	6060
I1	34001	4622
I2	23594	3866
J1	7372	2718
J2	12978	2185
K1	129674	5911
K2	59133	4107
L1	151565	6066
L2	0	0
M1	82059	8287
M2	46262	3740
N1	49664	5033
N2	4623	1434
O1	3481	404
O2	505	227
P1	52176	11684
P2	23522	9465
Q1	79341	14093
Q2	97472	12380
R1	116780	13809
R2	125308	8349
S1	62759	9977
S2	77581	13458
T1	36359	10742
T2	40821	8214

Sample	Mean VOL (Voxels)	Standard Deviation
U1	158894	16904
U2	61680	2341
V1	136747	8815
V2	43064	3674
W1	71696	6150
W2	319004	28868
X1	154316	3311
X2	74948	9718
Y1	27727	4895
Y2	4639	1413
Z1	62841	6773
Z2	59289	5201
AA1	251198	16277
AA2	66420	7483
AB1	238695	29519
AB2	165561	3310
AC1	95344	2698
AC2	21450	3461
AD1	13286	3807
AD2	4993	857
AE1	275231	11313
AE2	82788	10471

Sample	Days b/t Initiation of Tx and Post Op CBCT	Percentage Change in Lesion Size
B1, B2	355	100%
C1, C2	356	100%
D1, D2	146	-2%
E1, E2	299	-3%
F1, F2	151	85%
G1, G2	151	69%
H1, H2	151	80%
I1, I2	153	31%
J1, J2	153	-76%
K1, K2	153	54%
L1, L2	303	100%
M1, M2	322	44%
N1, N2	390	91%
O1, O2	119	85%
P1, P2	119	55%
Q1, Q2	98	-23%
R1, R2	98	-7%
S1, S2	307	-24%
T1, T2	307	-12%
U1, U2	91	61%
V1, V2	367	69%
W1, W2	241	-345%
X1, X2	315	51%
Y1, Y2	315	83%
Z1, Z2	136	6%
AA1, AA2	97	74%
AB1, AB2	91	31%
AC1, AC2	96	78%
AD1, AD2	96	62%
AE1, AE2	96	70%

Appendix E

Linear Measurements made by Radiologist (All measurements in mm)

Scan	Axial 1	Axial 2	Sagittal 1	Sagittal 2	Coronal 1	Coronal 2
B1	6.9	5.1	8.1	6.6	7.2	6.0
B2	0.0	0.0	0.0	0.0	0.0	0.0
C1	10.7	6.1	10.4	6.3	7.0	6.3
C2	4.4	3.5	-	-	4.3	2.0
D1	5.8	4.7	4.0	2.6	4.4	3.5
D2	5.1	4.7	5.8	3.7	4.5	1.6
E1	5.6	5.2	6.7	3.6	5.4	3.4
E2	5.6	5.1	6.1	3.0	5.3	2.4
F1	6.7	5.2	5.1	4.6	5.5	4.1
F2	4.0	2.9	3.8	2.0	3.1	2.3
G1	5.4	4.3	4.9	2.7	4.5	2.6
G2	2.6	2.3	3.9	1.4	-	-
H1	5.9	5.0	5.9	3.5	4.5	3.3
H2	-	-	-	-	-	-
I1	3.6	2.7	3.5	3.0	3.0	1.4
I2	2.2	2.0	3.2	0.8	-	-
J1	2.3	2.0	2.4	1.2	2.1	1.4
J2	2.3	1.9	2.1	1.2	2.2	1.6

Scan	Axial 1	Axial 2	Sagittal 1	Sagittal 2	Coronal 1	Coronal 2
K1	7.1	6.5	6.7	6.5	7.5	4.7
K2	4.5	4.3	-	-	-	-
L1	5.9	5.4	5.8	3.4	4.9	4.7
L2	-	-	-	-	-	-
M1	5.8	2.3	5.7	4.5	5.7	5.2
M2	5.1	2.1	4.5	4.0	-	-
N1	4.9	3.6	3.6	2.3	6.5	2.3
N2	2.0	1.9	3.0	1.0	2.2	0.9
O1	-	-	2.2	1.8	2.5	1.9
O2	-	-	-	-	-	-
P1	-	-	3.9	2.3	6.5	4.4
P2	-	-	-	-	-	-
Q1	7.5	4.7	5.1	4.7	7.0	6.2
Q2	5.5	4.1	-	-	5.5	5.1
R1	6.7	6.2	10.1	6.2	9.1	5.5
R2	6.5	6.2	10.0	6.0	7.7	5.5
S1	5.9	4.4	7.4	5.4	7.2	4.8
S2	5.5	4.9	7.8	6.1	7.1	5.3
T1	4.7	4.5	6.1	4.5	5.0	4.3
T2	4.8	4.1	5.2	5.1	5.0	4.5
U1	6.2	5.3	5.9	5.8	6.6	4.0
U2	4.7	4.1	4.0	2.8	5.1	2.6

Scan	Axial 1	Axial 2	Sagittal 1	Sagittal 2	Coronal 1	Coronal 2
V1	6.8	5.7	6.6	5.2	5.1	4.9
V2	5.7	5.1	4.1	3.8	4.1	3.8
W1	5.7	5.2	8.1	5.3	7.1	5.0
W2	13.2	9.8	8.8	5.6	12.0	6.2
X1	9.2	6.2	13.0	5.0	12.1	7.0
X2	5.0	2.2	6.5	5.5	6.9	4.8
Y1	7.9	6.0	9.0	5.1	9.5	7.3
Y2	6.4	6.0	-	-	9.2	7.3
Z1	6.5	6.2	7.3	5.9	7.3	3.4
Z2	6.4	6.1	6.5	4.9	-	-
AA1	7.9	5.7	10.5	6.1	11.9	7.4
AA2	4.3	2.5	3.4	1.9	4.5	1.7
AB1	10.4	8.1	8.6	8.2	9.6	7.9
AB2	10.1	6.2	6.4	5.2	8.1	3.5
AC1	5.2	5.0	5.5	5.1	6.2	2.4
AC2	-	-	3.2	1.5	3.7	1.8
AD1	-	-	2.3	1.5	-	-
AD2	-	-	-	-	-	-
AE1	7.9	6.1	6.4	4.9	7.1	6.9
AE2	-	-	4.6	2.5	4.3	2.0

Linear Measurements made by Endodontist
(All measurements in mm)

Scan	Axial 1	Axial 2	Sagittal 1	Sagittal 2	Coronal 1	Coronal 2
B1	7.3	6.1	8.3	7.0	7.0	6.8
B2	0.0	0.0	0.0	0.0	0.0	0.0
C1	10.3	7.9	11.2	6.0	7.4	5.9
C2	4.5	3.3	4.5	2.0	5.3	1.8
D1	3.7	2.0	5.3	3.0	4.5	3.7
D2	5.2	3.8	6.6	3.2	5.1	2.5
E1	5.8	5.8	6.9	5.8	5.8	4.9
E2	5.7	5.5	6.0	4.1	4.8	3.4
F1	6.7	5.9	6.1	4.1	5.1	5.0
F2	3.0	2.8	4.0	2.5	3.1	2.7
G1	6.3	3.8	4.3	4.0	3.6	3.3
G2	3.1	2.6	4.1	2.1	2.7	2.5
H1	7.0	4.6	7.5	5.6	4.2	3.8
H2	3.7	2.7	4.1	1.4	2.9	2.2
I1	4.3	3.1	3.6	2.6	3.4	2.0
I2	3.3	2.4	4.0	1.7	3.0	2.2
J1	2.0	2.0	2.3	1.7	2.2	1.6
J2	2.8	1.8	2.1	1.2	2.2	1.4

Scan	Axial 1	Axial 2	Sagittal 1	Sagittal 2	Coronal 1	Coronal 2
K1	7.5	6.8	6.4	6.2	7.7	6.3
K2	3.1	2.7	5.1	2.6	3.3	1.8
L1	6.2	5.5	5.4	4.7	6.9	6.5
L2	0.0	0.0	2.1	1.5	0.0	0.0
M1	5.2	2.9	6.5	2.9	5.6	4.8
M2	1.5	0.9	3.6	1.7	4.2	1.7
N1	5.5	1.2	3.8	3.5	6.1	3.9
N2	2.0	1.2	2.1	1.0	2.4	0.9
O1	2.0	1.5	2.5	1.1	3.4	2.3
O2	0.0	0.0	1.2	0.7	2.1	1.2
P1	3.8	3.2	6.4	3.2	3.9	2.8
P2	2.4	2.1	3.8	1.6	3.0	2.0
Q1	4.7	2.0	5.0	1.7	4.5	3.0
Q2	6.7	1.6	5.5	2.0	5.6	3.7
R1	7.5	6.2	11.0	6.5	7.4	6.8
R2	7.6	6.2	10.0	6.3	6.4	6.0
S1	6.5	5.0	8.4	5.4	8.0	4.3
S2	5.2	5.1	8.1	6.3	8.4	3.6
T1	5.0	4.7	8.4	5.1	4.7	4.3
T2	5.2	4.6	4.4	4.3	4.6	4.4
U1	6.7	4.6	5.3	5.1	6.4	5.8
U2	4.8	4.5	4.0	3.5	5.5	4.0

Scan	Axial 1	Axial 2	Sagittal 1	Sagittal 2	Coronal 1	Coronal 2
V1	6.0	5.6	8.1	6.0	5.3	5.2
V2	3.9	2.4	4.8	3.6	4.1	1.7
W1	5.2	2.7	8.7	3.1	8.0	3.3
W2	14.8	9.8	9.0	4.7	10.3	6.1
X1	6.5	3.1	12.1	3.3	8.2	6.7
X2	7.6	2.1	10.1	2.7	8.2	6.4
Y1	5.8	5.5	4.3	4.0	4.2	3.3
Y2	8.2	6.2	5.4	5.0	6.9	5.7
Z1	7.1	6.3	8.2	3.5	7.1	4.1
Z2	5.8	5.0	4.8	2.1	5.8	2.9
AA1	8.3	8.0	10.3	5.1	9.5	6.9
AA2	4.2	4.1	4.1	3.5	5.5	3.6
AB1	10.7	6.9	9.2	7.8	11.3	7.8
AB2	10.4	5.1	7.1	4.5	6.8	3.3
AC1	6.4	5.0	6.3	5.4	5.4	4.5
AC2	4.5	3.2	3.8	2.1	4.5	2.1
AD1	2.8	2.7	5.9	2.6	3.0	1.3
AD2	3.4	2.4	2.4	1.4	2.3	1.3
AE1	8.3	6.1	8.0	6.7	7.3	7.2
AE2	6.4	4.3	5.9	3.1	5.9	2.8

Appendix F

Likert Scale Recorded by Radiologist

1. I agree (no doubt or question) that this lesion is decreasing in size
2. I cannot say with any degree of certainty that this lesion is decreasing or increasing in size
3. I agree (no doubt or question) that this lesion is increasing in size

Scan	Change in Size
B	1
C	1
D	2
E	2
F	1
G	1
H	2
I	2
J	2
K	1
L	1
M	1
N	1
O	1
P	1
Q	1
R	2

Scan	Change in Size
S	3
T	3
U	1
V	1
W	3
X	2
Y	2
Z	2
AA	1
AB	1
AC	2
AD	2
AE	1

Likert Scale Recorded by Endodontist

1. I agree (no doubt or question that this lesion is decreasing in size
2. I cannot say with any degree of certainty that this lesion is decreasing or increasing in size
3. I agree (no doubt or question) that this lesion is increasing in size

Scan	Change in Size
B	1
C	1
D	3
E	2
F	1
G	1
H	1
I	2
J	2
K	1
L	1
M	1
N	1
O	1
P	1
Q	2
R	2

Scan	Change in Size
S	2
T	2
U	2
V	1
W	3
X	2
Y	3
Z	1
AA	1
AB	1
AC	1
AD	2
AE	1

References

1. Figdor D. Apical periodontitis: A very prevalent problem. *Oral Surg Oral Med Oral Pathol Oral Radiol Endod.* 2002 Dec;94(6):651-2.
2. Kakehashi S, Stanley HR, Fitzgerald RJ. The effects of surgical exposures of dental pulps in germfree and conventional laboratory rats. *J South Calif Dent Assoc.* 1966 Sep;34(9):449-51.
3. Moller AJ, Fabricius L, Dahlen G, Ohman AE, Heyden G. Influence on periapical tissues of indigenous oral bacteria and necrotic pulp tissue in monkeys. *Scand J Dent Res.* 1981 Dec;89(6):475-84.
4. Langeland K. Tissue response to dental caries. *Endod Dent Traumatol.* 1987 Aug;3(4):149-71.
5. Ricucci D, Langeland K. Apical limit of root canal instrumentation and obturation, part 2. A histological study. *Int Endod J.* 1998 Nov;31(6):394-409.
6. Ricucci D, Pascon EA, Ford TR, Langeland K. Epithelium and bacteria in periapical lesions. *Oral Surg Oral Med Oral Pathol Oral Radiol Endod.* 2006 Feb;101(2):239-49.
7. Thoma K. A histopathological study of the dental granuloma and diseased root apex. *J Natl Dent Assoc.* 1917;4:1075-90.
8. Ricucci D, Bergenholtz G. Histologic features of apical periodontitis in human biopsies. *Endod Topics.* 2004;8:68-87.
9. Ramachandran Nair PN, Pajarola G, Schroeder HE. Types and incidence of human periapical lesions obtained with extracted teeth. *Oral Surg Oral Med Oral Pathol Oral Radiol Endod.* 1996 Jan;81(1):93-102.
10. Ricucci D, Siqueira J. *Endodontology: An integrated biological and clinical view.* First ed. Quintessence Publishing; 2013.
11. Glickman GN. AAE consensus conference on diagnostic terminology: Background and perspectives. *J Endod.* 2009 Dec;35(12):1619-20.
12. Seltzer S, Bender IB, Ziontz M. The dynamics of pulp inflammation: Correlations between diagnostic data and actual histologic findings in the pulp. *Oral Surg Oral Med Oral Pathol.* 1963 Jul;16:846,71 contd.
13. Michaelson PL, Holland GR. Is pulpitis painful? *Int Endod J.* 2002 Oct;35(10):829-32.
14. Block RM, Bushell A, Rodrigues H, Langeland K. A histopathologic, histobacteriologic, and radiographic study of periapical endodontic surgical specimens. *Oral Surg Oral Med Oral Pathol.* 1976 Nov;42(5):656-78.
15. Lin L, Shovlin F, Skribner J, Langeland K. Pulp biopsies from the teeth associated with periapical radiolucency. *J Endod.* 1984 Sep;10(9):436-48.

16. Syrjanen S, Tammisalo E, Lilja R, Syrjanen K. Radiological interpretation of the periapical cysts and granulomas. *Dentomaxillofac Radiol.* 1982;11(2):89-92.
17. Lalonde ER. A new rationale for the management of periapical granulomas and cysts: An evaluation of histopathological and radiographic findings. *J Am Dent Assoc.* 1970 May;80(5):1056-9.
18. Kumar V, Abbas A, Fausto N, Aster J. Robbins and cotran pathologic basis of disease. 8th ed. ed. Saunders/Elsevier; 2010.
19. Gosain A, DiPietro LA. Aging and wound healing. *World J Surg.* 2004 Mar;28(3):321-6.
20. Guo S, Dipietro LA. Factors affecting wound healing. *J Dent Res.* 2010 Mar;89(3):219-29.
21. Strindberg L. The dependence of the results of pulp therapy on certain factors. *Acta Odontol Scand.* 1956;14(suppl 21):1-175.
22. Orstavik D. Time-course and risk analyses of the development and healing of chronic apical periodontitis in man. *Int Endod J.* 1996 May;29(3):150-5.
23. European Society of Endodontology. Quality guidelines for endodontic treatment: Consensus report of the european society of endodontology. *Int Endod J.* 2006 Dec;39(12):921-30.
24. Patel S, Durack C, Abella F, Shemesh H, Roig M, Lemberg K. Cone beam computed tomography in endodontics - a review. *Int Endod J.* 2015 Jan;48(1):3-15.
25. Eriksen HM, Orstavik D, Kerekes K. Healing of apical periodontitis after endodontic treatment using three different root canal sealers. *Endod Dent Traumatol.* 1988 Jun;4(3):114-7.
26. Murphy WK, Kaugars GE, Collett WK, Dodds RN. Healing of periapical radiolucencies after nonsurgical endodontic therapy. *Oral Surg Oral Med Oral Pathol.* 1991 May;71(5):620-4.
27. Goldman M, Pearson AH, Darzenta N. Endodontic success--who's reading the radiograph? *Oral Surg Oral Med Oral Pathol.* 1972 Mar;33(3):432-7.
28. Bender IB, Seltzer S. Roentgenographic and direct observation of experimental lesions in bone: I. 1961. *J Endod.* 2003 Nov;29(11):702,6; discussion 701.
29. Bender IB. Factors influencing the radiographic appearance of bony lesions. *J Endod.* 1997 Jan;23(1):5-14.
30. Shoha RR, Dowson J, Richards AG. Radiographic interpretation of experimentally produced bony lesions. *Oral Surg Oral Med Oral Pathol.* 1974 Aug;38(2):294-303.
31. Lee S, Messer H. Radiographic appearance of artificially prepared periapical lesions confined to cancellous bone. *Int Endod J.* 1986;19:64-72.
32. Huuonen S, Orstavik D. Radiological aspects of apical periodontitis. *Endod Topics.* 2002;1:3-25.

33. Paurazas SB, Geist JR, Pink FE, Hoen MM, Steiman HR. Comparison of diagnostic accuracy of digital imaging by using CCD and CMOS-APS sensors with E-speed film in the detection of periapical bony lesions. *Oral Surg Oral Med Oral Pathol Oral Radiol Endod.* 2000 Mar;89(3):356-62.
34. Velvart P, Hecker H, Tillinger G. Detection of the apical lesion and the mandibular canal in conventional radiography and computed tomography. *Oral Surg Oral Med Oral Pathol Oral Radiol Endod.* 2001 Dec;92(6):682-8.
35. Liang YH, Jiang L, Gao XJ, Shemesh H, Wesselink PR, Wu MK. Detection and measurement of artificial periapical lesions by cone-beam computed tomography. *Int Endod J.* 2014 Apr;47(4):332-8.
36. de Paula-Silva FW, Wu MK, Leonardo MR, da Silva LA, Wesselink PR. Accuracy of periapical radiography and cone-beam computed tomography scans in diagnosing apical periodontitis using histopathological findings as a gold standard. *J Endod.* 2009 Jul;35(7):1009-12.
37. Bender IB, Seltzer S. Roentgenographic and direct observation of experimental lesions in bone: II. 1961. *J Endod.* 2003 Nov;29(11):707,12; discussion 701.
38. Tsai P, Torabinejad M, Rice D, Azevedo B. Accuracy of cone-beam computed tomography and periapical radiography in detecting small periapical lesions. *J Endod.* 2012 Jul;38(7):965-70.
39. Lofthag-Hansen S, Huuonen S, Grondahl K, Grondahl HG. Limited cone-beam CT and intraoral radiography for the diagnosis of periapical pathology. *Oral Surg Oral Med Oral Pathol Oral Radiol Endod.* 2007 Jan;103(1):114-9.
40. Ahlowalia MS, Patel S, Anwar HM, Cama G, Austin RS, Wilson R, et al. Accuracy of CBCT for volumetric measurement of simulated periapical lesions. *Int Endod J.* 2013 Jun;46(6):538-46.
41. Patel S, Dawood A, Ford TP, Whaites E. The potential applications of cone beam computed tomography in the management of endodontic problems. *Int Endod J.* 2007 Oct;40(10):818-30.
42. Scarfe WC, Levin MD, Gane D, Farman AG. Use of cone beam computed tomography in endodontics. *Int J Dent.* 2009;2009:634567.
43. Cotton TP, Geisler TM, Holden DT, Schwartz SA, Schindler WG. Endodontic applications of cone-beam volumetric tomography. *J Endod.* 2007 Sep;33(9):1121-32.
44. Patel S, Dawood A, Whaites E, Pitt Ford T. New dimensions in endodontic imaging: Part 1. conventional and alternative radiographic systems. *Int Endod J.* 2009 Jun;42(6):447-62.
45. Scarfe WC, Farman AG, Sukovic P. Clinical applications of cone-beam computed tomography in dental practice. *J Can Dent Assoc.* 2006 Feb;72(1):75-80.
46. Kaffe I, Gratt BM. Variations in the radiographic interpretation of the periapical dental region. *J Endod.* 1988 Jul;14(7):330-5.
47. Barnett F. Cone beam-computed tomography in endodontics. Summer 2011 ENDODONTICS: Colleagues for Excellence newsletter. 2011.

48. Ludlow J. Dosimetry of the kodak 9000 3D small FOV CBCT and panoramic unit. *Oral Surg Oral Med Oral Pathol Oral Radiol Endod.* 2008;107:e29.
49. AAE and AAOMR joint position statement: Use of cone beam computed tomography in endodontics 2015 update. *J Endod.* 2015 Sep;41(9):1393-6.
50. Peters, C.I. and Peters, O.A. Cone beam computed tomography and other imaging techniques in the determination of periapical healing. *Endodontic Topics.* 2012;26:57-75.
51. Grondahl HG, Grondahl K, Webber RL. A digital subtraction technique for dental radiography. *Oral Surg Oral Med Oral Pathol.* 1983 Jan;55(1):96-102.
52. Webber RL, Ruttimann UE, Groenhuis RA. Computer correction of projective distortions in dental radiographs. *J Dent Res.* 1984 Aug;63(8):1032-6.
53. Cotti E, Campisi G, Ambu R, Dettori C. Ultrasound real-time imaging in the differential diagnosis of periapical lesions. *Int Endod J.* 2003 Aug;36(8):556-63.
54. Gundappa M, Ng SY, Whites EJ. Comparison of ultrasound, digital and conventional radiography in differentiating periapical lesions. *Dentomaxillofac Radiol.* 2006 Sep;35(5):326-33.
55. Nair MK, Seyedain A, Agarwal S, Webber RL, Nair UP, Piesco NP, et al. Tuned aperture computed tomography to evaluate osseous healing. *J Dent Res.* 2001 Jul;80(7):1621-4.
56. Nair MK, Nair UP, Seyedain A, Gassner R, Piesco N, Mooney M, et al. Correlation of tuned aperture computed tomography with conventional computed tomography for evaluation of osseous healing in calvarial defects. *Oral Surg Oral Med Oral Pathol Oral Radiol Endod.* 2007 Feb;103(2):267-73.
57. Ames JR, Johnson RP, Stevens EA. Computerized tomography in oral and maxillofacial surgery. *J Oral Surg.* 1980 Feb;38(2):145-9.
58. Velvart P, Hecker H, Tillinger G. Detection of the apical lesion and the mandibular canal in conventional radiography and computed tomography. *Oral Surg Oral Med Oral Pathol Oral Radiol Endod.* 2001 Dec;92(6):682-8.
59. Ahlowalia MS, Patel S, Anwar HM, Cama G, Austin RS, Wilson R, et al. Accuracy of CBCT for volumetric measurement of simulated periapical lesions. *Int Endod J.* 2013 Jun;46(6):538-46.
60. Whyms BJ, Vorperian HK, Gentry LR, Schimek EM, Bersu ET, Chung MK. The effect of computed tomographic scanner parameters and 3-dimensional volume rendering techniques on the accuracy of linear, angular, and volumetric measurements of the mandible. *Oral Surg Oral Med Oral Pathol Oral Radiol.* 2013 May;115(5):682-91.
61. van der Borden WG, Wang X, Wu MK, Shemesh H. Area and 3-dimensional volumetric changes of periapical lesions after root canal treatments. *J Endod.* 2013 Oct;39(10):1245-9.
62. Zhang MM, Liang YH, Gao XJ, Jiang L, van der Sluis L, Wu MK. Management of apical periodontitis: Healing of post-treatment periapical lesions present 1 year after endodontic treatment. *J Endod.* 2015 Jul;41(7):1020-5.

63. Metska ME, Parsa A, Aartman IH, Wesselink PR, Ozok AR. Volumetric changes in apical radiolucencies of endodontically treated teeth assessed by cone-beam computed tomography 1 year after orthograde retreatment. *J Endod.* 2013 Dec;39(12):1504-9.
64. Liang YH, Jiang LM, Jiang L, Chen XB, Liu YY, Tian FC, et al. Radiographic healing after a root canal treatment performed in single-rooted teeth with and without ultrasonic activation of the irrigant: A randomized controlled trial. *J Endod.* 2013 Oct;39(10):1218-25.
65. Estrela C, Bueno MR, Azevedo BC, Azevedo JR, Pecora JD. A new periapical index based on cone beam computed tomography. *J Endod.* 2008 Nov;34(11):1325-31.
66. Pope O, Sathorn C, Parashos P. A comparative investigation of cone-beam computed tomography and periapical radiography in the diagnosis of a healthy periapex. *J Endod.* 2014 Mar;40(3):360-5.
67. Liang YH, Li G, Wesselink PR, Wu MK. Endodontic outcome predictors identified with periapical radiographs and cone-beam computed tomography scans. *J Endod.* 2011 Mar;37(3):326-31.
68. Patel S, Wilson R, Dawood A, Foschi F, Mannocci F. The detection of periapical pathosis using digital periapical radiography and cone beam computed tomography - part 2: A 1-year post-treatment follow-up. *Int Endod J.* 2012 Aug;45(8):711-23.
69. Orstavik D, Kerekes K, Eriksen HM. The periapical index: A scoring system for radiographic assessment of apical periodontitis. *Endod Dent Traumatol.* 1986 Feb;2(1):20-34.
70. Mischkowski RA, Pulsfort R, Ritter L, Neugebauer J, Brochhagen HG, Keeve E, et al. Geometric accuracy of a newly developed cone-beam device for maxillofacial imaging. *Oral Surg Oral Med Oral Pathol Oral Radiol Endod.* 2007 Oct;104(4):551-9.
71. Whyms BJ, Vorperian HK, Gentry LR, Schimek EM, Bersu ET, Chung MK. The effect of computed tomographic scanner parameters and 3-dimensional volume rendering techniques on the accuracy of linear, angular, and volumetric measurements of the mandible. *Oral Surg Oral Med Oral Pathol Oral Radiol.* 2013 May;115(5):682-91.
72. Winberg T, Fouad A, Bennett I, Bellingham P, Otis L, Fouad A. A novel approach to the treatment and outcome assessment of apical periodontitis: A double-blind, randomized clinical trial. *JOE.* 2014 March;40(3):e2.
73. Goldman M, Pearson AH, Darzenta N. Reliability of radiographic interpretations. *Oral Surg Oral Med Oral Pathol.* 1974 Aug;38(2):287-93.
74. Simon JH. Incidence of periapical cysts in relation to the root canal. *J Endod.* 1980 Nov;6(11):845-8.
75. Nair PN. New perspectives on radicular cysts: Do they heal? *Int Endod J.* 1998 May;31(3):155-60.
76. Lin LM, Ricucci D, Lin J, Rosenberg PA. Nonsurgical root canal therapy of large cyst-like inflammatory periapical lesions and inflammatory apical cysts. *J Endod.* 2009 May;35(5):607-15.
77. Priebe WA, Lazansky JP, Wuehrman AH. The value of the roentgenographic film in the differential diagnosis of periapical lesions. *Oral Surg Oral Med Oral Pathol.* 1954 Sep;7(9):979-83.

78. Guo J, Simon JH, Sedghizadeh P, Soliman ON, Chapman T, Enciso R. Evaluation of the reliability and accuracy of using cone-beam computed tomography for diagnosing periapical cysts from granulomas. *J Endod.* 2013 Dec;39(12):1485-90.
79. Simon JH, Enciso R, Malfaz JM, Roges R, Bailey-Perry M, Patel A. Differential diagnosis of large periapical lesions using cone-beam computed tomography measurements and biopsy. *J Endod.* 2006 Sep;32(9):833-7.
80. Rosenberg PA, Frisbie J, Lee J, Lee K, Frommer H, Kottal S, et al. Evaluation of pathologists (histopathology) and radiologists (cone beam computed tomography) differentiating radicular cysts from granulomas. *J Endod.* 2010 Mar;36(3):423-8.
81. Nair PN, Sjogren U, Figdor D, Sundqvist G. Persistent periapical radiolucencies of root-filled human teeth, failed endodontic treatments, and periapical scars. *Oral Surg Oral Med Oral Radiol Endod.* 1999 May;87(5):617-27.
82. Lin LM, Rosenberg PA. Repair and regeneration in endodontics. *Int Endod J.* 2011 Oct;44(10):889-906.
83. Love RM, Firth N. Histopathological profile of surgically removed persistent periapical radiolucent lesions of endodontic origin. *Int Endod J.* 2009 Mar;42(3):198-202.
84. Schulz M, von Arx T, Altermatt HJ, Bosshardt D. Histology of periapical lesions obtained during apical surgery. *J Endod.* 2009 May;35(5):634-42.
85. Christiansen R, Kirkevang LL, Gotfredsen E, Wenzel A. Periapical radiography and cone beam computed tomography for assessment of the periapical bone defect 1 week and 12 months after root-end resection. *Dentomaxillofac Radiol.* 2009 Dec;38(8):531-6.
86. Petersson A, Axelsson S, Davidson T, Frisk F, Hakeberg M, Kvist T, et al. Radiological diagnosis of periapical bone tissue lesions in endodontics: A systematic review. *Int Endod J.* 2012 Sep;45(9):783-801.
87. Fristad I, Molven O, Halse A. Nonsurgically retreated root filled teeth--radiographic findings after 20-27 years. *Int Endod J.* 2004 Jan;37(1):12-8.
88. Molven O, Halse A, Fristad I, MacDonald-Jankowski D. Periapical changes following root-canal treatment observed 20-27 years postoperatively. *Int Endod J.* 2002 Sep;35(9):784-90.

Vita

Dr. Jeremy Ward Fike was born on February 4, 1983 in Memphis, Tennessee and is an American citizen. Dr. Fike received his Bachelor of Science in Biochemistry from Abilene Christian University in 2005 and Doctor of Dental Surgery from the Texas A&M University Baylor College of Dentistry in 2011. He subsequently received a Certificate in Advanced Education in General Dentistry from the Olin E. Teague Veterans' Center in Temple, Texas in 2012. Dr. Fike then entered private practice in Temple, Texas and completed two years in general dental practice. In 2014, he enrolled in the Advanced Specialty Program in Endodontics at Virginia Commonwealth University School of Dentistry. Dr. Fike is a member of the American Association of Endodontists, American Dental Association, and Texas Dental Association. He will graduate with a Master of Science in Dentistry and a Certificate in Endodontics.